Astronomy & Astrophysics manuscript no. BMP_resub
November 14, 2016

Something borrowed, something blue: The nature of blue metal-poor stars inferred from their colours and chemical abundances ⋆

C. J. Hansen[1,2], P. Jofré[3,4], A. Koch[2], A. McWilliam[5], and C. S. Sneden[6]

[1] Dark Cosmology Centre, The Niels Bohr Institute, Juliane Maries Vej 30, DK-2100 Copenhagen, Denmark
[2] Department of Physics, Lancaster University, Bailrigg, Lancaster LA1 4YB, UK
[3] Institute of Astronomy, University of Cambridge, Madingley Road, Cambridge CB3 0HA, United Kingdom
[4] Núcleo de Astronomía, Facultad de Ingeniería, Universidad Diego Portales, Av. Ejército 441, Santiago, Chile
[5] Carnegie Observatories, 813 Santa Barbara St., Pasadena, CA 91101, USA
[6] Department of Astronomy, University of Texas at Austin, 1 University Station C1400, Austin, TX 78712, USA

ABSTRACT

Blue metal-poor stars (BMPs) are main sequence stars that appear bluer and more luminous than normal turnoff stars. They were originally singled out by using $B-V$ and $U-B$ colour cuts. Early studies found that a larger fraction of field BMP stars were binaries compared to normal halo stars. Thus, BMP stars are ideal field blue straggler candidates for investigating internal stellar evolution processes and binary interaction. In particular, the presence or depletion in lithium in their spectra is a powerful indicator as to their origin. They are either old, halo blue stragglers experiencing internal mixing processes or mass transfer (Li-depletion), or intermediate-age, single stars of possibly extragalactic origin (2.2 dex halo plateau Li). However, we note that internal mixing processes can lead to an increased level of Li. Hence, this study combines photometry and spectroscopy to unveil the origin of various BMP stars. We first show how to separate binaries from young blue stars using photometry, metallicity, and lithium. Using a sample of 80 BMP stars (T> 6300K), we find that 97% of the BMP binaries have $V-Ks_0 < 1.08 \pm 0.03$, while BMP stars that are not binaries lie above this cut in 2/3 of the cases. This cut can help classify stars which lack radial velocities from follow-up observations. We then trace the origin of two BMP stars from the photometric sample by conducting a full chemical analysis using new high-resolution and high signal-to-noise spectra. Based on their radial velocities, Li, α, and s- and r-process abundances we show that BPS CS22874-042 is a single star (A(Li)= 2.38 ± 0.10 dex) while with A(Li)= 2.23 ± 0.07 dex CD-48 2445 is a binary, contrary to earlier findings. Our analysis emphasises that field blue stragglers can be segregated from single metal-poor stars, using $(V-Ks)$ colours with a fraction of single stars polluting the binary sample, but not vice versa. These two groups can only be properly separated by using information from stellar spectra, illustrating the need for accurate and precise stellar parameters and high resolution, high S/N spectra in order to fully understand and classify this intriguing class of stars. Our high-resolution spectrum analysis confirms the findings from the colour cuts and shows that CS 22874−042 is single, while CD −48 2445 most likely is a binary. Moreover, the stellar abundances show that both stars formed in situ; CS 22874−042 carry traces of massive star enrichment and CD −48 2445 shows indications of AGB mass transfer mixed with gases ejected possibly from neutron star mergers.

Key words. Stars: abundances — stars: blue stragglers — stars: fundamental parameters — stars: Population II — Galaxy: abundances — Galaxy: halo

1. Introduction

Amongst the many intriguing facets of the Galactic halo, the near-constancy in lithium abundance, at A(Li)=2.2 dex over a broad range in temperature and metallicity (the so-called "Spite-plateau"), is now a well-established property of old and warm halo main-sequence stars (Spite & Spite 1982). Thus, a star presenting lithium abundances that deviate from the plateau value, either through strong enhancements or depletions, suggests that it has experienced internal or external alterations that are not present in its halo star counterparts, motivating us to investigate these physical processes that have changed its lithium abundance.

Metal-poor dwarfs depleted in lithium are relatively common (e.g., Sbordone et al. 2010) and one option is that they have suffered from mass transfer or merging between stars (e.g., Carney et al. 2005). On the other hand, there are far fewer cases of metal-poor dwarfs which have Li abundances significantly higher than the plateau value (Deliyannis et al. 2002; Asplund et al. 2006; Koch et al. 2011; Monaco et al. 2012), and it is still not clear how these form. Possible explanations include diffusion within the star (Richard et al. 2005), seeding by supernovae (SNe; Woosley & Weaver 1995), asymptotic giant branch (AGB) companions (Ventura & D'Antona 2011), or accretion of substellar bodies (Ashwell et al. 2005).

Blue stragglers are excellent candidates to learn about the processes that can create and destroy lithium in main-sequence stars. These stars can obtain their blue colour and low Li in a number of ways; through mass transfer, coalesence, pulsational driven mass loss or internal mixing, where mass transfer seems to be the preferred scenario (Preston & Sneden 2000). Hence,

Send offprint requests to:
C. J. Hansen, e-mail: cjhansen@dark-cosmology.dk
⋆ Based on UVES archive data 077.B-0507 and 090.B-0605. This paper includes data gathered with the 6.5 meter Magellan Telescopes located at Las Campanas Observatory, Chile.

blue stragglers are bluer than turn-off stars of a coeval population because they became more massive thanks to direct mass transfer from a companion star in a binary system. If mass transfer has taken place a higher rotation velocity will often testify to this, and Li will subsequently be destroyed. The binary system will typically consist of two low-mass stars, where one of them is a white dwarf ($< 0.55 M_{\odot}$ on an almost circular orbit with a period of a few hundred days (Carney et al. 2005)). Thus, spectroscopic studies of blue stragglers in the halo help to investigate processes of mass transfer, which Li excellently traces (Carney et al. 2005). In this study, we therefore present analyses of photometry and spectroscopy, as both are needed to pin down the true origin of the BMP stars.

Contrary to globular clusters, field blue stragglers are difficult to find because of the variety of metallicities and distances that stars in the Galactic halo cover. Although the inner halo is composed of one dominant co-eval population, presenting a well-defined turn-off colour as a function of metallicity (e.g., Preston et al. 1991; Unavane et al. 1996; Jofré & Weiss 2011), not all main-sequence stars that are bluer than this turn-off temperature are necessarily blue stragglers. They could also be intermediate-age stars with extragalactic origin that were accreted later onto the Milky Way (Preston et al. 1991; Unavane et al. 1996), or simply warm, metal-poor single stars formed in situ. In this context, the radial velocity variations and the abundance of lithium give key information about the nature of BMP stars: while blue stragglers should present overall, strong modifications of their Li-content, intermediate-age stars should be Li-normal (Ryan et al. 2001). To determine if the star has an extra-galactic origin, the $\alpha-$abundances are useful discriminants (see, e.g., Nissen & Schuster 2010) and Hansen et al. 2016).

The largest sample of BMP stars to date is still the one published 16 years ago by Preston & Sneden (2000, hereafter PS00). The stars were selected using a $B-V$ vs. $U-B$-diagram. PS00 analysed a sample of 62 BMP stars using high-resolution, low signal-to-noise ratio (SNR$\sim$ 10 – 30) spectroscopy and monitored their radial velocities (RVs) over seven years. From this, Sneden et al. (2003) found a systematic difference in the $s-$process enhancement between stars with constant and varying radial velocities (RV). The study of PS00 also revealed that 17 stars had constant RV and more than 50% of them were low in $\alpha-$elements, and thus good contenders for intermediate-age, accreted stars. The Li abundances in these intermediate-age candidates have not been studied so far.

It is important to note that the Li resonance line at 6707.8 Å becomes very weak in BMP stars, where an abundance at the Spite-Plateau value of A(Li)=2.2 produces an equivalent width (EW) of less than 10 mÅ (Preston 2015). Furthermore, one needs to be aware that a lithium abundance alone is not a clear discriminator between (Li depleted) blue stragglers and intermediate-age, metal-poor dwarfs with (generally) a normal Li abundance. For instance, in the Hyades, dwarfs with similar temperatures to the BMP stars in PS00 are depleted in Li, producing the so-called “Li-dip" (Boesgaard & Tripicco 1986). Carney et al. (2005) addressed this issue and showed that one BMP star, at constant RV in the temperature range of the Li-dip (between 6400 and 6800 K) is depleted in Li by ~0.7 dex while another star had normal plateau value. These authors suggested that, at low metallicities, the temperature range of the Li-dip could be shifted towards hotter temperatures, or that no Li-dip exists at low metallicities. However, Asplund et al. (2006) and Bonifacio et al. (2007) found a first indication for this feature among metal-poor Population II stars, which they relate to effects of mass loss on the main sequence, as predicted by Dearborn et al. (1992).

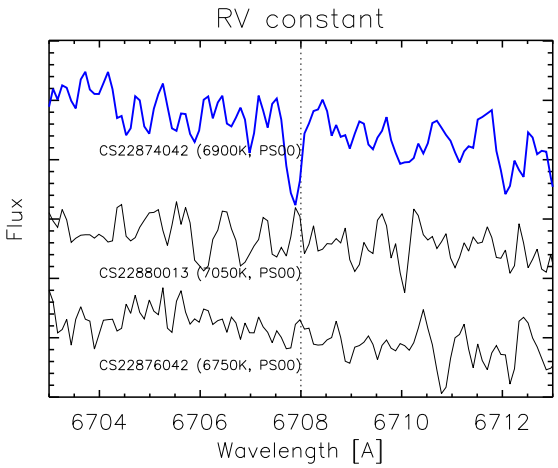

Fig. 1. Spectrum taken from PS00 of the star CS 22874−042 around the Li line at 6707.8 Å. Stars with similar temperatures (according to PS00) shown for comparison.

In this work, we aim to gain insights into to possible mechanisms that can alter the Li abundances in field blue stragglers or BMP stars. Therefore, we need to perform not only a Li abundance analysis of the BMP stars but also a detailed spectral analysis of $\alpha-$, r- and s-process elements. The former two allow us to investigate a Galactic vs. extragalactic origin and exact formation site, while s-element abundances provide information on the presence and amount of mass transfer from a binary AGB companion star. The latter scenario can also be tested through possible RV variations and change in colour. The PS00 sample is an obvious starting point as they provide information on radial velocities, $\alpha-$ and s-process abundances. Unfortunately, their spectra were of too low signal-to-noise to confidently allow for Li and r-element detections in these warm, dwarf stars. This prompted the need for high SNR spectra.

The RV-constant star, CS 22874-024, turned out to be an outlier in PS00 as it showed a notable Li line of $\sim$ 26 mÅ (see Fig. 1). According to the stellar parameters of CS 22874-024 reported in PS00, this would correspond to an abundance of A(Li) = 3.25, which is significantly higher than the Spite-plateau value, as well as the value expected from Big Bang Nucleosynthesis (BBN; Cyburt et al. 2008). High resolution, high SNR spectra are clearly needed to confirm the stellar parameters and accurately measure key tracer abundances from weaker lines.

We compile a large sample of 80 BMP stars from the literature to devise a method to separate blue stragglers from metal-poor single stars based on various properties. In particular, we show that their Li and heavy element abundances plus their colours are imperative to segregate the BMP stars in subsamples (§2). In §3 we introduce a subsample of stars including BMP and benchmark stars, for which we derive detailed chemical abundances. The results from our spectral analysis are presented in §4, which we discuss in §5 before concluding our results in §6.

2. Photometry of the BMP sample

Here we select warm stars (T> 6300K) with gravities around or above 4.0 dex spanning a broad range of metallicities for a sample consisting of both binaries and single stars with known Li abundances to develop a way of separating single and binary

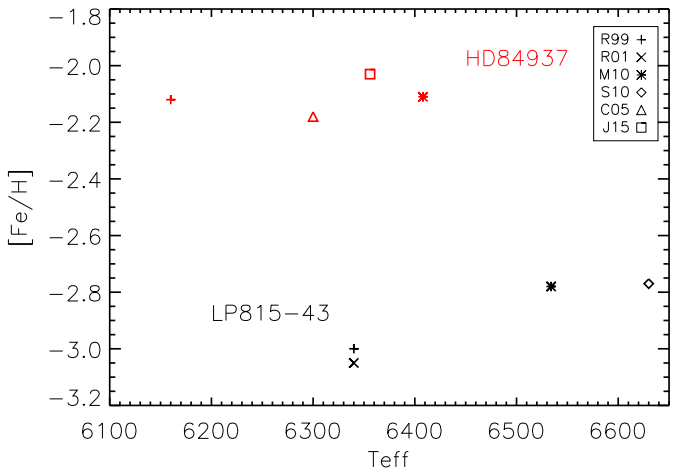

Fig. 2. Temperature and [Fe/H] for two well-studied stars HD84937 and LP815-43 Ryan et al. (1999, R99), Ryan et al. (2001, R01), Carney et al. (2005, C05), Meléndez et al. (2010, M10), Sbordone et al. (2010, S10), and Jofré et al. (2015, J15).

blue stars. This temperature range is selected so that a possible Li gap may be detected if existing for these field BMP stars.

The sample listed in Table 1 and 2 is composed of stars from large samples presenting various levels of Li (Ryan et al. 1999; Preston & Sneden 2000; Ryan et al. 2001; Carney et al. 2005; Asplund et al. 2006; Bonifacio et al. 2007; Meléndez et al. 2010; Sbordone et al. 2010). We intentionally choose studies that have an overlap in order to gain a better handle on the systematic offsets among the different methods they employ. We also include some of the well-studied Gaia-ESO Survey benchmark stars (Heiter et al. 2015a; Jofré et al. 2014), and explore how the temperature scales offset the Li abundances. An example of this is shown in Fig. 2 where two stars (LP 815−43 and HD 84937) show temperatures that span ∼ 250 K while their [Fe/H] is better constrained (within ±0.2 dex). For A(Li) in HD84937 (Meléndez et al. 2010, T=6408K) a value of 2.32 is derived, while the study by Ryan et al. (1999) obtained a lower temperature (T= 6160 K) and in turn a lower A(Li)= 2.17. This means that 250 K is enough to shift the lithium abundance above or below the Spite plateau (Spite & Spite 1982), but it stays within the uncertainty of Li abundances on the plateau (∼ 0.09 dex according to Bonifacio et al. 2007).

2.1. Li and $V - Ks$ as binary/BMP segregators

Since our compilation of Li abundances relies on literature, we note that the different methods employed may shift the results by up to 250 K or ∼ 0.2 dex in A(Li). This abundance offset arises because the derived Li value heavily depends on the effective temperature; a parameter that differs when derived from phometry (IRFM) to spectroscopy (e.g., Hα-fitting), and both of these methods have been used in the studies we compare to. Hence, to lower this impact of temperature on the absolute value of A(Li) we turn towards photometry and study the direct impact of the star's blue colour, and later connect this to the lithium abundance (through stellar spectroscopy). Based on the average uncertainties in photometry (±0.01 mag) and dereddening (0.01 – 0.1 mag) taken from the same literature as the BMP sample (e.g., Meléndez et al. 2010; Ryan et al. 2001). A typical uncertainty of 0.01 mag translates into ∼ 50 K. We probe

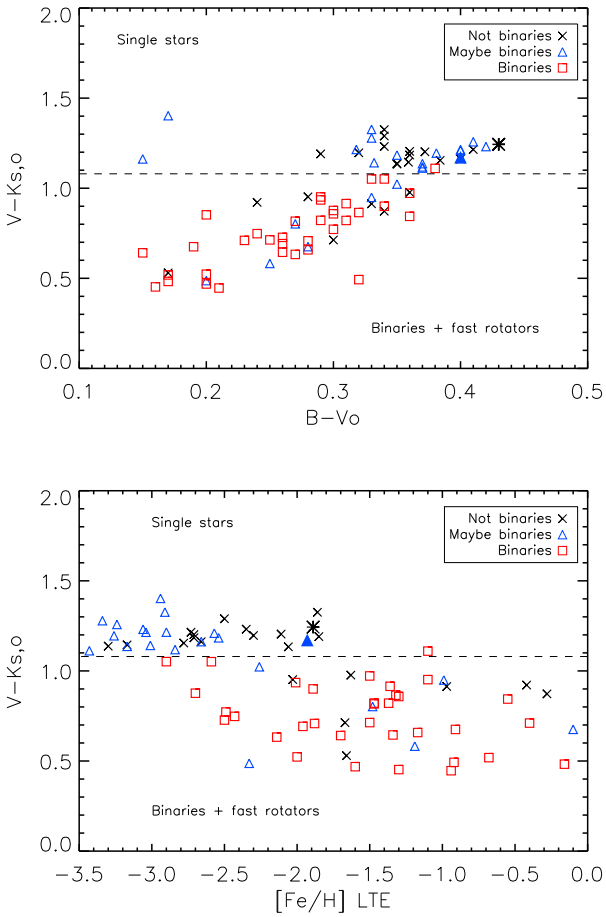

Fig. 3. Dereddened $B - V$ vs $V - K_s$ (top) and $V - K_s$ vs [Fe/H] (bottom) for binaries (red squares), maybe binaries (blue triangles) and single stars (black X). A separation (dashed line) between single stars and binaries is show for $V - Ks_0 = 1.08$. CS 22874−042 is shown as an asterisc and CD −48 2445 is indicated by a larger, filled triangle.

the trends using $U - B, B - V, V - Ks$, and the dereddened values $U - B_0, B - V_0, V - Ks_0$. These colours can be calculated for the majority of BMP stars studied here. The cleanest trends and best way of categorising the BMP stars into groups is obtained using $B - V_0$ and $V - Ks_0$. The sample of 80 stars distributed amongst binaries (34 stars, red squares), single stars (23, black 'x'), and possible binaries (tagged 'maybe' owing to a lack of repeat radial velocity measurements amounts to 23 stars, blue triangles). The V magnitudes are taken from the respective studies while the 2MASS K_s magnitudes are based on the SIMBAD references. The dereddening, $E(B-V)$, is based on literature when provided, otherwise it is the mean S& F (Schlafly & Finkbeiner 2011) from the IRSA webpage[1]. Their colour-metallicity distribution is shown in Fig. 3. This figure surprisingly shows that all but one binary star fall below $V - Ks_0 = 1.08$. This corresponds to 97% of the binary stars falling below this cut with a pollution of 1/3 of the single stars. A similar, but less clean finding is made for $B - V_0$. We note that a linear relationship between the sum of the three Ca line equivalent widths and the metallicity in a globular cluster was discovered by Armandroff & Zinn (1988) using integrated light spectroscopy. With this in mind, we see that simple metallicity indicators such as the near-IR Ca triplet

[1] http://irsa.ipac.caltech.edu/applications/DUST/

Table 1. Coordinates, photometry (from Simbad and literature), dereddening, temperature, metallicity, Li abundance, radial velocity (RV), and literature reference for the binary and candidate binary BMP sample. An '*' indicates that the star was analysed spectroscopically in this study. Our values are listed in Tables 3, 5, and 7.

Star	Ra(α), Dec(δ) (J2000.0)	V [mag]	Lit. V [mag]	K_s [mag]	E(B-V) [mag]	T [K]	[Fe/H] dex	A(Li) dex	RV [km/s]	Ref.
Binaries										
BD+51 1817	13 08 39.10, +51 03 59.26	10.21	10.23	9.08	0.000	6345	−1.10	1.64	...	R01
BD+25 1981	08 44 24.69, +24 47 47.75	9.29	9.29	8.39	0.000	6780	−1.30	1.75	...	R01
BD+23 74	00 32 43.32, +24 13 21.41	9.88	9.88	9.11	0.022	7500	−0.91	1.32	32.5	C05
G202−65	16 35 58.58, +45 51 59.26	11.06	11.22	10.18	0.000	6390	−1.50	1.67	...	R01
HD8554	01 24 42.30, +07 00 05.23	9.57	9.57	8.63	0.030	6780	−1.47	1.11	11.1	C05
HD109443	12 34 46.73, −23 28 32.20	9.25	9.25	8.16	0.077	6650	−0.55	0.67	43.4	C05
HD135449	15 16 10.39, −32 53 33.03	9.46	9.46	8.15	0.285	6740	−0.92	1.10	−42.0	C05
CS22956−028	21 44 48.72, −63 22 09.80	13.00	13.00	11.98	0.028	7035	−1.89	2.00	...	L05, PS00
CS29497−030	00 40 47.93, −24 07 33.91	12.66	12.70	11.75	0.014	6650	−2.70	1.10	...	S04, PS00
CS22873−139	20 05 55.15, −59 17 11.40	13.83	13.80	12.63	0.030	6400	−2.90	2.15	...	R01
CS22166−004	00 52 11.44, −11 04 40.06	13.08	13.10	12.53	0.028	....	−1.30	....	...	PS00
CS22166−041	01 10 56.36, −13 42 43.50	14.36	14.30	13.34	0.020	7050	−1.32	....	...	PS00
CS22170−028	00 51 07.37, −11 08 31.95	11.52	11.80	11.17	0.027	8050	−0.68	....	...	PS00
CS22174−040	01 28 40.52, −07 24 04.30	13.18	13.20	12.62	0.026	....	−1.60	....	...	PS00
CS22872−062	16 26 37.03, −04 32 54.06	14.05	14.30	12.86	0.200	7900	0.24	....	...	PS00
CS22874−034	14 38 26.84, −23 14 48.49	14.49	14.60	13.66	0.095	....	−1.70	....	...	PS00
CS22876−008	23 55 21.37, −34 48 01.30	13.95	13.90	13.12	0.012	7200	−1.88	....	...	PS00
CS22876−021	00 01 03.78, −33 48 15.76	14.48	14.50	13.48	0.011	7250	−1.10	....	...	PS00
CS22880−073	20 48 10.95, −20 59 23.90	14.05	14.10	13.19	0.058	....	−0.40	....	...	PS00
CS22885−048	20 19 53.78, −38 56 36.07	14.27	14.30	13.21	0.050	7050	−1.36	....	...	PS00
CS22890−069	15 24 12.28, +03 05 06.43	12.71	12.70	12.03	0.039	....	−2.00	0.00	...	PS00
CS22894−029	23 42 14.62, −00 51 32.71	14.37	14.40	13.48	0.023	7350	−1.47	....	...	PS00
CS22896−149	19 43 44.92, −56 10 08.76	13.03	12.10	11.47	0.040	7950	−0.16	0.00	...	PS00
CS22941−005	23 29 52.83, −35 13 03.83	14.61	14.60	13.77	0.016	7450	−2.43	....	...	PS00
CS22946−011	01 19 11.68, −19 23 58.12	13.95	14.00	12.87	0.014	6850	−2.59	....	...	PS00
CS22948−068	21 49 06.93, −37 27 52.49	13.77	13.70	12.78	0.022	7200	−1.37	....	...	PS00
CS22963−013	02 53 53.75, −06 42 17.84	13.51	13.50	12.61	0.045	....	−2.50	....	...	PS00
CS22966−037	23 43 38.60, −31 48 18.40	14.02	14.00	13.28	0.013	7400	−1.34	....	...	PS00
CS22966−043	23 43 54.45, −28 18 34.50	13.56	13.60	12.83	0.014	7300	−1.96	....	...	PS00
CS22966−054	23 49 51.58, −29 08 21.45	14.43	14.40	13.65	0.019	7250	−1.17	....	...	PS00
CS29509−027	00 50 15.78, −30 59 56.16	12.72	12.50	11.47	0.019	7050	−2.01	....	...	PS00
CS29518−024	01 17 12.12, −32 26 57.79	14.52	14.50	13.96	0.020	7650	−0.94	....	...	PS00
CS29518−039	01 22 45.58, −28 24 29.84	14.26	14.20	13.35	0.014	7050	−2.49	....	...	PS00
CS29527−038	00 37 44.69, −20 08 11.12	14.41	14.40	13.60	0.017	....	−1.50	....	...	PS00
CS29527−045	00 35 50.90, −17 57 00.57	14.04	14.00	13.28	0.019	7250	−2.14	....	...	PS00
Maybe binaries										
BD+24 1676	07 30 41.26, +24 05 10.25	10.80	10.80	9.54	0.013	6387	−2.54	2.27	−238.6	R99,M10
CD−24 17504	23 07 20.23, −23 52 35.60	12.18	12.18	10.81	0.020	6451	−3.34	2.18	136.6	M10
CD−33 01173	03 19 35.32, −32 50 43.14	10.90	10.94	9.75	0.005	6536	−3.01	2.18	47.6	R99,M10
CD−48 2445*	06 41 26.66, −48 13 14.95	10.54	10.54	9.29	0.015	6453	−1.93	2.22,2.38	319.2	M10,A06
G064−12	13 40 02.50, −00 02 18.80	11.45	11.45	10.21	0.003	6463	−3.26	2.32	442.5	R99,M10
HD338529	19 32 31.91, +26 23 26.14	9.37	9.37	8.14	0.060	6335	−2.26	2.25	−128.3	A06
LP831−070	03 06 05.43, −22 19 17.94	11.80	11.80	10.34	0.005	6414	−2.94	2.28	−48.2	R99,M10
BS16023−46	14 00 54.47, +22 46 42.34	14.23	14.23	12.96	0.004	6547	−2.90	2.27	...	M10,B07,S10
BS17570−63	00 20 36.19, +23 47 37.70	14.51	14.51	13.07	0.026	6318	−2.91	2.06	...	M10,B07,S10
BS17572−100	09 28 55.35, −05 21 40.38	12.19	12.19	10.95	0.016	6596	−2.66	2.28	191.0/189.0	M10,B07,S10
CS22177−009	04 07 40.64, −25 02 43.94	14.27	14.27	12.95	0.023	6421	−3.04	2.28	−1.9	M10,B07,S10
CS22888−031	23 11 32.47, −35 26 42.90	14.90	14.90	13.58	0.007	6335	−3.24	2.11	−126.0	M10,B07,S10
CS22953−037	01 25 06.65, −59 16 00.70	13.64	13.64	12.46	0.008	6532	−2.84	2.27	−153.0	M10,B07,S10
CS22966−011	23 35 07.05, −30 22 54.35	14.55	14.55	13.28	0.000	6307	−3.06	1.92	...	M10,B07,S10
CS29518−043	01 18 38.30, −30 41 02.66	14.57	14.57	13.37	0.008	6517	−3.17	2.20	...	M10,B07,S10
CS29527−015	00 29 10.68, −19 10 07.25	14.24	14.24	13.05	0.014	6541	−3.43	2.25	48.0	M10,B07,S10
CS31061−032	02 38 43.29, +03 19 02.44	13.90	13.90	12.61	0.015	6433	−2.57	2.23	...	M10,B07,S10
CS22174−008	01 11 45.47, −10 40 03.81	13.62	13.60	12.69	0.025	7320	−1.48	....	...	PS00
CS22896−103	19 33 15.47, −54 58 52.01	14.54	14.50	13.66	0.046	7400	−0.10	....	...	PS00
CS29497−017	00 31 25.75, −23 57 26.82	14.14	14.10	13.44	0.014	7500	−1.19	....	...	PS00
CS29499−057	23 51 32.25, −25 45 46.53	13.85	13.80	13.22	0.019	7700	−2.33	....	...	PS00
CS29517−021	23 58 09.09, −14 51 47.30	13.60	13.60	12.54	0.027	7000	−0.99	....	...	PS00

Notes. References: R99: Ryan et al. (1999), PS00: Preston & Sneden (2000), R01:, Ryan et al. (2001), S04: Sivarani et al. (2004), C05: Carney et al. (2005), L05: Lucatello et al. (2005), A06: Asplund et al. (2006), B07: Bonifacio et al. (2007), M10: Meléndez et al. (2010), S10: Sbordone et al. (2010).

Table 2. Coordinates, photometry (from Simbad and literature), dereddening, temperature, metallicity, Li abundance, radial velocity (RV), and literature reference for the single star BMP sample. An '*' indicates that the star was analysed spectroscopically in this study. Our values are listed in Tables 3, 5, and 7.

Star	Ra(α), Dec(δ) (J2000.0)	V [mag]	Lit. V [mag]	K_s [mag]	E(B-V) [mag]	T [K]	[Fe/H] dex	A(Li) dex	RV [km/s]	Ref.
Single stars										
BD+03 0740	04 55 43.46, +31 09 00.93	10.76	9.80	9.51	0.022	6419	−2.71	2.21	174.2	R99,A06,M10
BD+09 2190	09 29 15.56, +08 38 00.46	11.14	11.15	9.91	0.015	6392	−2.66	2.13	266.6	R99,A06
BD−13 3442	11 46 50.65, −14 06 43.45	10.27	10.29	9.02	0.011	6311	−2.71	2.16	116.1	R99,A06
CD−3514849	21 33 49.75, −35 26 14.23	10.63	10.57	9.29	0.002	6396	−2.35	2.37	108.0	R99,A06,M10
G064−37	14 02 30.09, −05 39 05.20	11.14	11.14	9.92	0.012	6583	−3.17	2.21	81.5	R99,M10
HD84937	09 48 56.10, +13 44 39.32	8.32	8.32	7.06	0.005	6408	−2.11	2.32	−15.0	M10,C05
HD142575	15 55 02.84, +05 04 12.15	8.62	8.62	7.51	0.056	6550	−0.97	1.45	−65.0	C05
LP815−43	20 38 13.30, −20 26 10.87	10.72	10.91	9.65	0.024	6534	−2.78	2.26	−3.6	S10,M10,A06
CS22874−042*	14 38 01.94, −24 58 44.32	13.91	13.91	12.42	0.076	6500/6900	−1.90	2.38	176.0	Our,PS00
CS22950−173	20 35 31.26, −15 53 30.60	14.04	14.04	12.66	0.046	6353	−2.73	2.21	69.0	S10,PS00
CS22964−214	20 05 50.00, −39 27 43.30	13.66	13.70	12.32	0.076	6340	−3.30	2.15	...	R01,PS00
CS22175−034	02 20 21.52, −10 38 08.95	12.60	12.60	11.62	0.024	7100	−0.28	....	...	PS00
CS22185−009	03 14 53.75, −14 43 53.71	13.79	13.80	12.93	0.043	7100	−1.67	....	...	PS00
CS22871−040	14 39 20.00, −20 50 31.62	12.72	12.80	11.99	0.087	7880	−1.66	....	...	PS00
CS22874−009	14 34 23.17, −26 17 37.62	13.58	13.70	12.53	0.077	7600	−0.42	....	...	PS00
CS22876−042	00 12 00.83, −33 59 50.50	13.12	13.10	11.90	0.011	6750	−2.06	....	...	PS00
CS22880−058	20 43 55.98, −21 36 32.50	14.54	14.60	13.25	0.043	7150	−1.85	....	...	PS00
CS22941−012	23 28 29.73, −32 48 46.40	12.45	12.50	11.47	0.013	7200	−2.03	....	...	PS00
CS22948−079	21 47 29.21, −39 25 19.26	13.72	13.70	12.62	0.024	6700	−1.63	....	...	PS00
CS22950−078	20 24 57.80, −16 29 57.70	14.62	14.70	13.19	0.053	6900	−1.86	....	...	PS00
CS22950−173	20 35 31.26, −15 53 30.60	14.04	14.10	12.66	0.039	6800	−2.50	....	...	PS00
CS22960−058	22 16 05.87, −42 26 42.80	13.50	13.50	....	0.012	6900	−1.99	....	...	PS00
CS22964−074	19 49 29.42, −39 42 39.40	14.46	14.50	13.12	0.055	6950	−2.30	....	...	PS00

Notes. References: R99: Ryan et al. (1999), PS00: Preston & Sneden (2000), R01:, Ryan et al. (2001), C05: Carney et al. (2005), A06: Asplund et al. (2006), M10: Meléndez et al. (2010), S10: Sbordone et al. (2010).

(CaT) combined with photometry can be used as a first approach to sort blue stars into binaries and single stars as well as classifying possible binary candidates into one of these two groups (without needing follow-up observations).

However, these trends become stronger and cleaner once A(Li) is considered. Figure 4 shows A(Li) as a function of $V - Ks_0$ with a very clean separation of binaries below 1.08 and single stars above this colour cut. From the same figure binaries are seen to fall below the Spite plateau (green long dashed line) while the most metal-poor, single stars are seen to cluster around the Spite plateau, and mainly reside above $V - Ks_0 = 1.08$ (see top panel in Fig. 4). The trend is clean and the contamination is low (1 out of 39 stars does not follow the trend). This confirms that Li is a useful measurement to separate BMP stars into blue stragglers and metal-poor, single stars (Carney et al. 2005). This method is a very promising tool using $V - Ks_0 = 1.08$ and the Spite plateau as segregators of binary stars. A slight increase in [Fe/H] with decreasing $V - Ks_0$ is seen in the bottom panel of Fig. 4.

Now considering A(Li) as a function of temperature we find outliers above and below the Spite plateau. The Li melt-down from Sbordone et al. (2010) using IRFM in concordance with the methods employed by most studies shown here seem to need a strong downward shift in both Li and [Fe/H] to match these BMP stars. These are less prominent when A(Li) is plotted vs [Fe/H] (see Fig. 5). The three stars with the highest A(Li) in Table 1 and 2 according to Meléndez et al. (2010) are: CD −35 14849, CD −48 2445, and CS 22874−042 (shown by a larger asterisc). However, Asplund et al. (2006) report a lower Li abundance (2.22 dex) for CD −48 2445 and several of the other stars that overlap between the two studies. Our analysis support the lower values and we therefore only conduct a spectrum analysis the latter two of the three stars, a possible binary and a single star, to investigate their formation mechanism. Another outlier is the single star HD142575, which Carney et al. (2005) explained by a high rotational velocity decreasing the Li abundance so that it in our classification could be mistaken as a binary star. This makes blue fast rotating stars possible contaminators in our colour-separation method. Thus, in the following we look into the impact of rotation and the existence of the so-called Li gap or dip (see, e.g., Boesgaard & Tripicco 1986, and Sect. 5.1).

Using the colour cut and Li we thus select CD −48 2445 and HD 142575 as comparison stars. In our high SNR spectroscopic analysis we use their abundances to explore differences and similarities in their formation compared to that of CS 22874−042.

3. Spectrum analysis of extreme BMP and benchmark stars

Here we define a high Li abundance value (Li-rich) as A(Li)> 2.3 dex (Spite Plateau plus typical uncertainty ∼ 0.09 dex) in very metal-poor stars with T> 6300 K. Meanwhile, we will refer to Li-normal as 2.2 and Li-low as < 2.1 dex. To place the analysis of CS 22874−042 in context, we will in the following also consider two other BMP stars for comparison: HD 142575 (Li poor), and CD −48 2445 (Li rich, see Fig. 5 according to Meléndez et al. (2010)). The photometric properties are summarised in Table 3. A short recap of stars we compare to in our spectroscopic study is presented in Table 5. These stars are the outliers or most extreme BMP stars tagged in Fig. 5.

3.1. CS 22874−042

The spectrum from PS00 is plotted in Fig. 1 and corresponds to 22 stacked, individual exposures. It clearly shows a strong

Table 3. Photometric data of the three stars employed in our analysis as taken from Simbad. B and V magnitudes are on the Johnson Cousin system. For CS 22874−042 they were taken from Beers et al. (2007) while for CD −48 2445 and HD 142575 the values were taken from Simbad. All JHK_s magnitudes are from the 2MASS catalog, and reddening mean values from Schlafly & Finkbeiner (IRSA, 2011).

Star	RA (J2000.0)	DEC (J2000.0)	B	V	J	H	K_s	E($B-V$)
CS 22874−024	14 38 01.7	−24 58 47	14.34	13.91	12.77	12.48	12.42	0.076
CD −48 02445	06 41 26.7	−48 13 15	10.94	10.54	9.59	9.34	9.29	0.071
HD 142575	15 55 02.8	+05 04 12	9.00	8.62	7.72	7.56	7.51	0.056

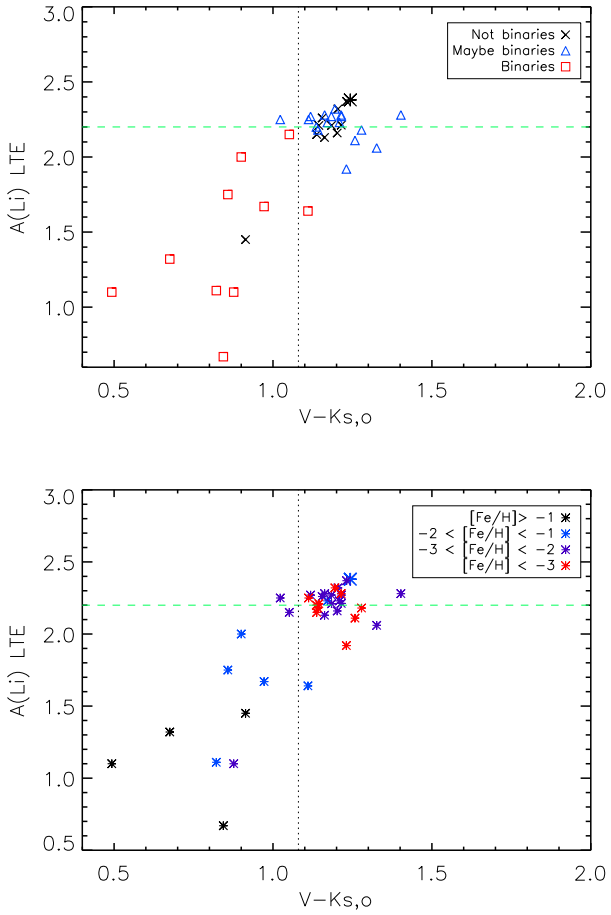

Fig. 4. A(Li) vs dereddened $V-Ks$ (legend as in Fig. 3. Binaries are separated from single stars by $V-Ks_0$=1.08 and the Spite plateau. The same sample is colour coded by metallicity (bottom panel). Values for CD −48 2445 and CS 22874−042 are from this study with CS 22874−042 shown as a larger asterisc.

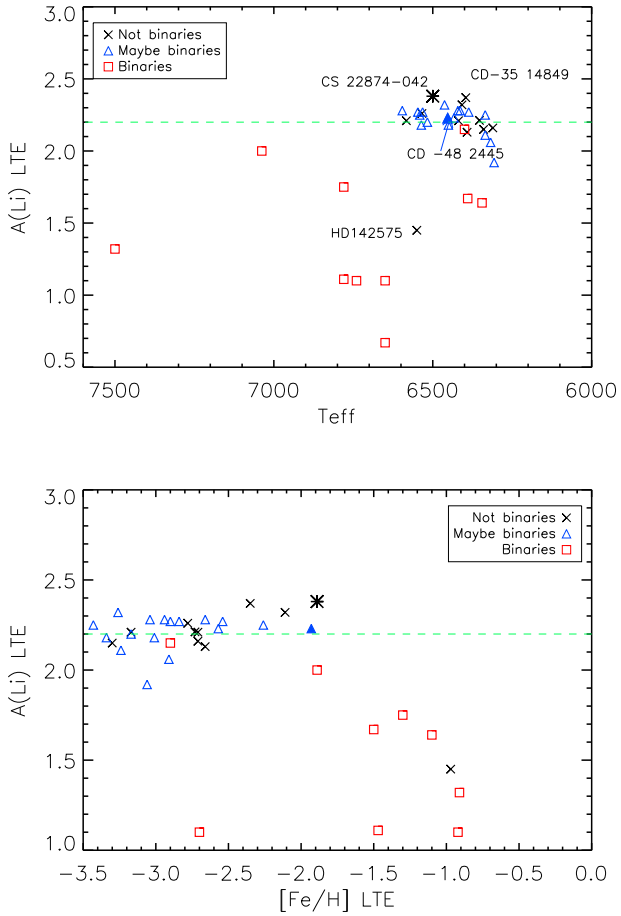

Fig. 5. A(Li) vs T and [Fe/H] (legend as in Fig. 3. Except from one case, the binaries do not reach the Spite plateau.

Li feature highlighting our interest in follow-up observations of this Li-rich BMP star (according to our convention see Sect.3). A high-resolution spectrum of CS22874-042 was obtained on 19/20, August, 2014, using the MIKE echelle spectrograph on the 6.5m Clay telescope at Las Campanas Observatory. We employed a 0.5x5.0" slit and 2x1 binning of the CCD pixels. Three exposures were obtained, in order to better eliminate cosmic-ray events, for a total integration time of 3000 sec. During the first two exposures the guide camera seeing was 0.53", fwhm, but for the third integration the seeing worsened somewhat, ranging from 0.67 to 0.89" fwhm.

The MIKE CCD data were reduced using the pipeline developed by Kelson (2003). The final blue side spectrum provided continuous wavelength coverage from 3360 Å to 5000 Å , at a resolving power of R ~57,000. At the peak of the orders in the blue-side spectrum, a S/N of 66 per pixel was obtained near 5000 Å, increasing to maximum of 98 per pixel at 4679 Å, and then steadily declining: at 4000 Å S/N=64, while at 3364 Å S/N=9 per pixel.

The red side spectrum provided continuous coverage from 4950 Å to 9400 Å, with a resolving power of R~48,000. The S/N peaked near 100 per pixel at 8590 Å, slowly declining with decreasing wavelength: a S/N=87 per pixel was obtained at the peak of the H_α order, 76 per pixel in the Na D order, and 52 per pixel in the Mg b order.

The RV of CS 22874−042 was re-determined by cross-correlating the spectrum with a template of HD 84937 using the code `iSpec` (Blanco-Cuaresma et al. 2014a). We used this star as template because its stellar parameters (Jofré et al. 2014; Heiter et al. 2015a) are similar to this BMP star. Moreover,

we have a high-resolution and high-SNR spectrum covering the entire optical range (see Blanco-Cuaresma et al. 2014b, for details). The RV obtained from this was 178.5±0.6 km s^{-1} and is fully consistent with the values reported by PS00 > 14 years ago. This consolidates the fact that this star has no significant RV variations, confirming its purported origin as a metal-poor, single, blue star. Owing to its α−enhancement ([α/Fe] = 0.35) it seems unlikely that this star should be an accreted star. We look further into the formation of this star in Sect. 4 and Sect. 5.

3.2. CD −48 2445

This star has been included as a comparative star as its stellar parameters are very similar to the parameters we derived for CS 22874−042 (see Sect. 4.1). We adopted the stellar parameters from Meléndez et al. (2010) who reported $T_{\rm eff}$=6453 K, log g=4.25, [Fe/H]= −1.93, $v_{\rm mic}$=1.5 km s^{-1} and A(Li) = 2.38 when assuming local thermodynamical equilibrium (LTE). In the following we compute all stellar abundances using these parameters. We note that Asplund et al. (2006) found lower values for the temperature and Li in this star. We therefore check if the absoprtion lines (including the Balmer lines) are well fit with the higher adopted temperature in order to reassess the Li value (see Table 5, Fig. 6, and Sect. 4.2 for further details on our derived abundances.

The spectrum of this star has been obtained with the UVES instrument in the BLUE346 and REDL580 settings in November 2012[2] and thus its reduced spectrum is publicly available. The SNR is 60 per pixel in the blue and 100 in the red part, and the resolution is of 60,000. We corrected its RV using `iSpec` in the same way as for CS 22874−042 obtaining a heliocentric velocity of 305 ± 0.23 km s^{-1} for CD −48 2445.

The spectrum analysed in Asplund et al. (2006) was taken in 2002 and the authors derived an RV of 319.2 ± 0.3 km s^{-1} and noted that this star showed no evidence of having a companion, while Ryan & Norris (1991) measured an RV of 338 ± 7 km s^{-1} and Augensen (1979) reported an RV of 301 ± 1.4 km s^{-1} determined from a spectrum taken in 1976. Taking the combined uncertainties into account (< 10 km s^{-1}, CD −48 2445 seems be a binary star given the difference of 37 km s^{-1} over the 40 years timespan between these different works. Our colour cut ($V - Ks_0$ = 1.08) confirms the suggested binary nature of CD −48 2445. Hence, we look into mass transfer signatures in Sect. 5.2 as this star is an excellent candidate of a binary system now containing a low-mass (< 0.55M$_\odot$) white dwarf.

3.3. HD 142575

This star has been included in this analysis because it is part of the RV constant (− 65km s^{-1}) BMP stars from Carney et al. (2005), with measured Li abundance of A(Li) = 1.45; it has a temperature of 6700 K placing it within the Li-dip. This BMP star has a rotational velocity of *vsini* = 13.0 km s^{-1} and a metallicity of −0.97 dex (Carney et al. 2005). The spectrum of this star was obtained with the UVES instrument with the in BLUE346, REDL580 and REDL860 gratings in 2006-06-11[3].

[2] Programme ID: 090.B-0605
[3] Programme ID: 077.B-0507

4. Stellar parameters and abundances

In this section we present the new results from our stellar parameter determination and the spectral analysis of the two BMP stars under study.

4.1. New atmospheric parameters of CS 22874−042

From our new spectra we re-determined the stellar parameters and, while we found different parameters from PS00, we still support the view that this CS 22874−042 is a BMP star. Since the final Li abundance is very sensitive to the effective temperature, we determined the stellar parameters using various methods. We considered photometry for the $T_{\rm eff}$, ionisation and excitation equilibrium from the EWs of iron lines, as well as synthesis of several spectral features such as the Mg triplet and the Balmer wings, and various iron line profiles. A summary of our results can be found in Table 4. Not all temperature or gravity indicators are equally good and we therefore assign weights to the methods we employ. Here we use values between 1 (full weight) and 0 (method discarded) to indicate the fraction with which the value enters the final averaged value. Below we describe each of these analyses in greater detail.

Photometric effective temperature: We used three different Infrared Flux Method (IRFM) calibrations to determine the temperature, namely Casagrande et al. (2010), Ramírez & Meléndez (2005), and (Alonso et al. 1996) for dwarfs and subgiants. These methods have also been used in the literature samples we compared to. We calculated the effective temperature using different colours ($B-V$, $V-K$, $J-K$), employing the three calibrations mentioned above, where applicable. The reddening E($B-V$) was found in the IRSA Dust maps of Schlafly & Finkbeiner (2011) and Schlegel et al. (1998), and we calculated the temperature using both (mean) values (0.075 mag for CS 22874−042 and 0.0878 mag for CD −48 2445). This lead to an E($B-V$) difference of ∼ 0.01 mag which translates into a temperature uncertainty of ∼ 50 K. We therefore round off all photometric temperatures to the nearest 50K. The values listed in Table 4 are based on the E($B-V$) from Schlafly & Finkbeiner (2011) and the B, V photometry from Beers et al. (2007) and 2MASS from Skrutskie et al. (2006).

Effective temperature from wings of Balmer lines: With `iSpec` we determined $T_{\rm eff}$ using the wings of the Balmer lines: H$_\alpha$, H$_\beta$, H$_\gamma$ and H$_\delta$. The results can be seen in Table 4. As expected, NLTE effects are important for metal-poor dwarfs, and depending on the stellar parameters the LTE temperature from, e.g., Hα may be a few percent too low (typically 50-100 K; Barklem 2007).

Surface gravity from Mg triplet: The surface gravity of our target was confirmed with `iSpec` by fitting the Mg triplet lines. For this determination we tested different values of effective temperature and metallicity around our accepted value of 6500 K and −1.8 dex, respectively (see below). In all cases the gravities yielded between 4.3 and 4.6, supporting the gravity of 4.5 reported in PS00. This rules out the possibility of our star being a BHB or an RR Lyrae star, which have lower gravities.

Parameters from iron line syntheses: We used the `iSpec` code to fit 150 Fe lines (amongst them, 17 lines are of the ionised species) ranging from 3440 to 7900 Å. For the regions outside the line list used within the Gaia-ESO Survey (Heiter et al.

Table 4. Stellar parameters of CS 22874−042 derived in different ways. The photometric temperatures were derived using Casagrande et al. (2010) - C10, Ramírez & Meléndez (2005) - RM05, and (Alonso et al. 1996) - A96. Method *b* is iterated to a stronger/smaller uncertainty than *a*.

Parameter	Values	Tag/Comment	Weight
T_{ex}	6500/ 6550/6850	a/b/PS00	1/0/0
$T_{H\delta}$	6600	-	1
$T_{H\gamma}$	6450	-	1
$T_{H\beta}$	6350	log$g$ sensitive	0
$T_{H\alpha}$	6250	log$g$ sensitive	0
T_{B-V}	6700/6450/6600	C10/A96/RM05	1/0/0
T_{V-K_s}	6300	A96	1
T_{J-K_s}	6450	C10	1
T_{final}	6500 ± 100		
logg_{Fe}	4.5		0.8
logg_{Mg}	4.6		0.2
logg_{final}	4.5 ± 0.1		
[FeI/H]	−1.95		0.5
[FeII/H]	−1.91		0.5
$[Fe/H]_{final}$	−1.9 ± 0.1		
V_{mic}	1.9 ± 0.1 km/s	Fe I lines	
Vsin$i$	2.7 ± 0.3 km/s	Profile matching	
RV_{helio}	178.5 ± 0.6 km/s	Cross correlation	

Table 5. Stellar parameters and Li-abundance of the stars we compare to with values taken from literature. An '*' indicates 3D analysis.

star	Teff (K)	logg (dex)	[Fe/H] (dex)	vmic (km/s)	vsini (km/s)	A(Li)	Reference
BPS CS22874−042	6500	4.5	−1.9	1.9	2.7	2.38	This work
BPS CS22874−042	6900	4.5	−1.53	2.0	8.0	–	PS00
CD −48 2445	6222/6453	4.25/4.25	−1.93/ − 1.93	1.5/1.5	2.3*/–	2.22/2.38	A06/M10
HD 142575	6550/6700	–/3.6	−0.97/ − 0.9	–/1.7	13.0	1.45	C05/F00
HD 106038	5905/5950	4.3/4.3	−1.35/ − 1.44	1.2/1.1	0.5/-	2.48/–	A06/H12
HD 84937	6356/6300	4.06/–	−2.03/ − 2.18	1.3/-	5.2/4.8	2.23	J15/C05
BPS CS 22950−173	6335/6506	4.2/4.5	−2.78/ − 2.61	1.4/1.4	–	2.20	S10 (min/max)
LP 815−43	6453/6630	3.8/4.1	−2.88/ − 2.77	1.7/1.7	– / –	2.23/2.16	S10/A06

Notes. References: F00: Fulbright (2000), PS00: Preston & Sneden (2000), C05: Carney et al. (2005), A06: Asplund et al. (2006), M10: Meléndez et al. (2010), S08: Smiljanic et al. (2008), S10: Sbordone et al. (2010), H12: Hansen et al. (2012), J15: Jofré et al. (2015).

2015b), we considered the atomic information provided by VALD (Kupka et al. 2011), as provided in the wrapper of `iSpec`. This method is based on a large number of lines and we therefore assign the resulting temperature the largest weight. By fixing $\log g = 4.5$ we obtained a temperature of 6500 K and a metallicity of −1.8 dex. When letting $\log g$ vary we obtained a slightly lower temperature of ∼6450 K, but recovered the same metallicity and a gravity of 4.2.

Parameters from equivalent widths of iron lines: For this test we used Fe lines below 5000Å from Hansen et al. (2012). In total 35 Fe I lines ($\sigma_{[\mathrm{Fe\ I/H}]} = 0.1$ dex) and 15 Fe II ($\sigma_{[\mathrm{Fe\ II/H}]} = 0.06$ dex) lines were used to determine the stellar parameters. Of these, 19 Fe I lines and 8 Fe II lines overlap with the lines in PS00. For most of the Fe I lines the atomic data agrees to the third digit with their line list values, but for the Fe II lines there is a (slight) difference in $\log gf$ values. This difference can be up to 0.05 but is in most cases around 0.01 or below. The EWs were measured in normalised spectra using IRAF, and the stellar parameters were determined by manually interpolating them in MOOG (Sneden 1973), the same spectrum synthesis code as used in PS00, but here adopting a more recent version (v. 2014).

The temperature was set by requiring that all Fe lines give the same Fe abundance regardless of excitation potential. The interpolation was stopped when the slope of the trend was less than ±0.05 dex/K. A similar approach, enforcing ionisation equilibrium between abundances from Fe I and Fe II, was applied to fix the gravity. Once the Fe I and II abundances agreed within 0.05 dex, the iteration stopped. Since ionisation balance is easily achieved and the lines show a low internal line-to-line scatter (∼ 0.1 dex) in good agreement with the `iSpec` line synthesis method. The metallicity was adopted as an average of all Fe I and II abundances (as these agree owing to the forced ionisation and excitation equilibrium). Finally, the microturbulence was determined minimizing the equivalent width trend with Fe II abundances, allowing for a variation in slope of up to ±0.05 dex/km s^{-1}. The spectroscopically constrained parameters with this method are (T_{eff}, $\log g$, [Fe/H], v_{mic}): 6550K, 4.5 dex, −1.9 dex, 1.9 km s^{-1} (see Table 4).

The constrained set of values agree well with the averaged photometric values. However, this temperature is still lower than what was found in PS00. Therefore, we carried out the same analysis using only the Fe lines and atomic data from PS00. When using their lines (38 Fe I and 8 Fe II) we find a $\log g$ value that agrees to within 0.1 dex, a [Fe/H] within 0.07 dex, and a

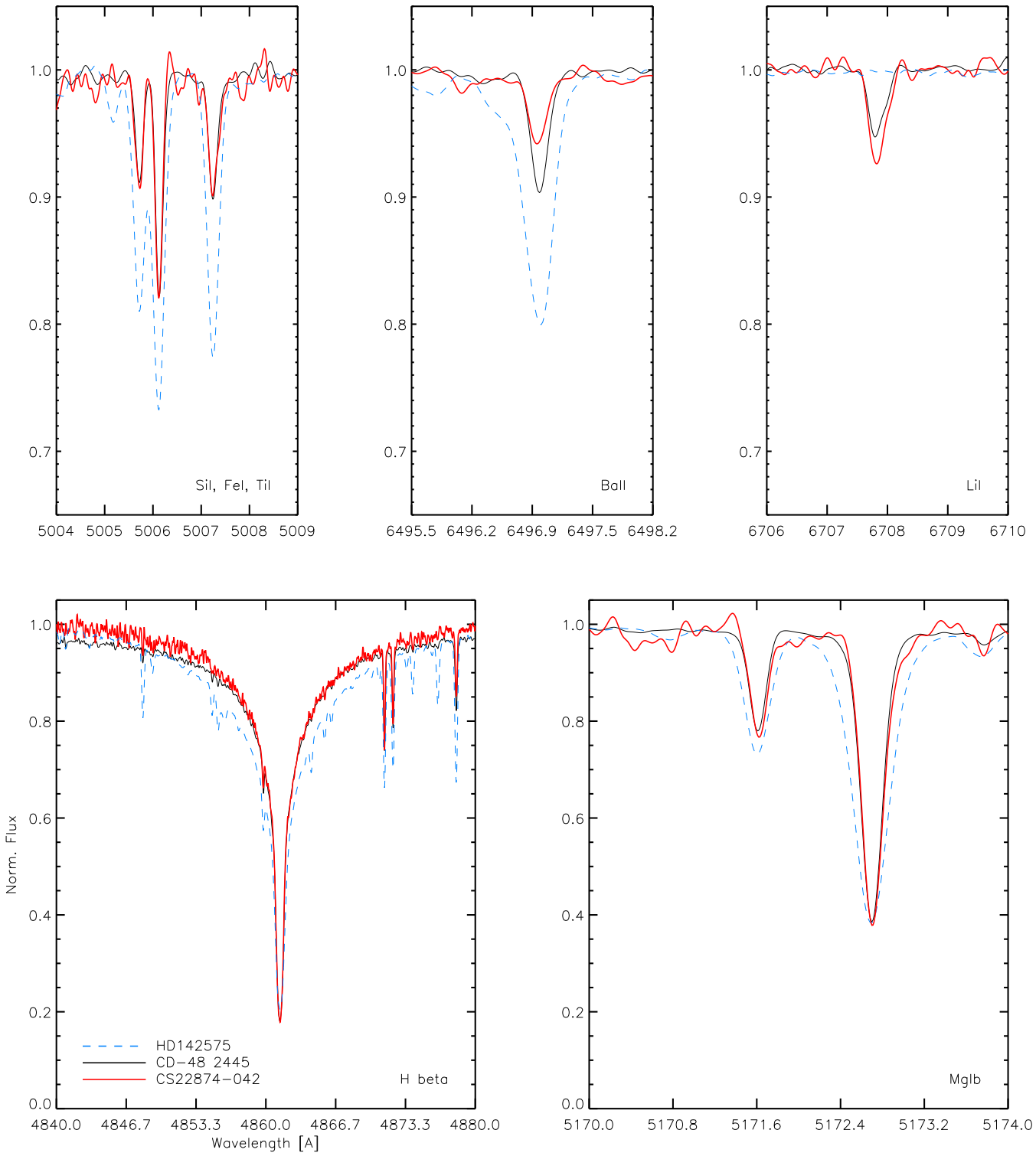

Fig. 6. Illustrative line profiles in different regions of the spectra. The stellar parameters of CD −48 2445 and CS 22874−042, as well as α−abundances are comparable, while the abundance of Ba and Li are different. HD 142575 has a higher metallicity, temperature and rotational velocity with respect to the other BMP stars. Li in this star can not be measured here.

$T_{\rm eff}$ within 50 K compared to their published values. The $v_{\rm mic}$ agrees within 0.1 km s^{-1}. The choice of lines, spectrum quality, and continuum placement lead to the slight differences in EWs, and in turn abundances, which can explain the differences we find. We note that the spectroscopic temperature may be biased by the few low excitation Fe I lines measurable.

In summary, we derived the fiducial set of stellar parameters ($T_{\rm eff}$/log g/[Fe/H]/$v_{\rm mic}$/v sin i): 6500±100 K/4.5±0.1 dex/−1.9±0.1 dex/1.9±0.1 km s^{-1}/2.7±0.3 km s^{-1}. The stated v sin i could be a placeholder for an unre-

Table 6. Line list used in our analysis. Full version available online, a portion is shown here for guidance.

Wavelength [Å]	Species	$\log gf$	E.P. [eV]	Reference
7771.940	8.0	0.370	9.140	WIE
7774.170	8.0	0.220	9.140	WIE
7775.390	8.0	0.000	9.140	WIE
4057.505	12.0	−1.201	4.343	SNE
4167.271	12.0	−1.004	4.343	SNE
4702.991	12.0	−0.666	4.343	SNE
5528.405	12.0	−0.620	4.343	SNE
...	...	...	...	...

Notes. References correspond to WIE: Wiese et al. (1996); SNE: Sneden et al. (2014), LAW: Lawler et al. (2001a,b); SOB: Sobeck et al. (2007); YAN: Yan et al. (1998).

solved macroturbulence. With these low velocities and the limitation in spectrum quality, we cannot distinguish between v sin *i* and v_{macro}. The summary of the different results can be found in Table 4.

We note that the parameters of CD −48 2445 (see Sect. 3.2) are very similar to our final ones for CS 22874−042 ($\sim \pm 50$K, 0.25, 0.03, 0.4km s^{-1}). Their similar parameters can be confirmed in Fig. 6, where we plot some regions of the spectra of the three BMP stars, sensitive to stellar parameters as described in Sect. 3. The wings of the Balmer line indicate that the temperatures of CS 22874−042 and CD −48 2445 are comparable, while the temperature of HD 142575 is higher. The wings of the Mg line also confirm that the surface gravities of all stars are those of dwarfs, since lower gravities create narrower Mg wings. In the top left panel we plot the profiles of three (Fe, Si and Ti) lines . This shows that CS 22874−042 and CD −48 2445 not only have comparable stellar parameters, but also $\alpha-$ and iron-peak abundances which allows for a very direct comparison of the derived abundances in CS 22874−042 and CD −48 2445. The main differences between the chemical composition of these two stars are found for the heaviest (s-process) and lightest (Li) elements under study (see Ba and Li panel of Fig. 6).

4.2. Chemical abundance determination

We derived the abundances of 17 elements that display detectable lines in the covered wavelength range of the spectrum of CS 22874−042. The abundances were derived using MOOG and the line lists from Sneden et al. (2014); the atomic data are given in the online Table A.1. The results for the final abundances of both stars are listed in Table 7.

Among the 17 element of which we measured abundances, Mg, Ca, Sc, Ti, Cr, Mn, Sr and Ba have been measured by PS00 for CS 22874−042 as well. Contrary to PS00, we find an $\alpha-$enhancement of CS 22874−042 normal of metal-poor halo stars ([α/Fe]= 0.35 ± 0.09), while PS00 found that CS 22874−042 was '$\alpha-$poor' ([α/Fe] ∼ 0.2) and thus a good candidate for an (intermediate-age) star with extragalactic origin. This is due to the lower temperature and metallicity determined by us with respect to the values of PS00. Regarding the iron-peak elements Sc, Cr and Mn, we obtain a slight enhancement of [Sc/Fe] = 0.3 dex and [Cr/Fe] = 0.2 dex, while PS00 obtained a similar enhancement for Sc but an underabundance of Cr of −0.15 dex. This can be due to differences in line lists like hyperfine splitting or other updates such as line blends. However, we mainly assign this to the better SNR of our new spectrum around the Cr lines compared to PS00. Manganese is similarly underabundant in both studies. Finally, regarding the heavy *s*−process elements Ba and La, we obtain a good agreement of Ba abundances with solar values while La is only an upper limit. A moderate enhancement for Sr is derived, in contrast to PS00 who obtained [Sr/Fe] = −0.4. This is in part due to the updated atomic data we used for Sr (Bergemann et al. 2012; Hansen et al. 2013) and in part owing to the different stellar parameters and spectrum quality especially in the blue wavelength range.

With our higher quality spectrum, we were able to measure elements that were not reported by PS00, namely Li, O, Na, Al, Si, V, Co, Ni, Y, and Zr. Like Mn, Al is underabundant. As for La and Ba, a slight weak *s*−process enhancement is found for Sr, Y, and Zr. Silicon and oxygen behave like the rest of the $\alpha-$elements, that is, with the normal enhancement of halo stars, and Co and Ni have solar values. An interesting case is V, which, at 0.3 dex, is rather enhanced for an iron-peak element. The line, however, is weak, noisy, and the abundance should be treated with caution.

Finally, the most surprising abundance value is that of Li with A(Li) = 2.38±0.10 dex, which remains enhanced with respect to Spite plateau value, even after our re-determination of the stellar parameters. While recent studies attest to an increasing Li with increasing metallicity, studies of globular clusters at similar metallicity to this star find a very homogeneous Li-abundance; e.g., NGC 6397 at [Fe/H]=−2.0 dex shows A(Li)=2.25 (Lind et al. 2009) over a broad range of evolutionary stages. In the metal-poor regime, Bonifacio et al. (2007) state a 1σ-scatter in A(Li) of 0.09 dex so that CS22874-042 can in fact be considered a 2σ outlier (modulo our measurement error).

Furthermore, the star presents no detectable *r*−process element lines in its spectrum. This may however be an observational bias owing to the fact that the star is a hot dwarf preventing us from detecting, e.g., the Eu, Sm, Gd, and Dy lines. For example, the EW of the generally strong Eu line at 4129 Å lies below 3 mÅ at these stellar parameters for a solar Eu abundance. This is at the noise level of our spectrum and thus, detecting very low abundances of Eu for our BMP star is not possible within our spectrum.

For the comparison star, CD −48 2445, the Li abundances have been reported in the literature, with a plateau value of 2.2 (Asplund et al. 2006) to 2.38 (Meléndez et al. 2010). In comparison we derive an A(Li) of 2.23 agreeing well within the combined errors with the measurement of Asplund et al. (2006). Here we report abundances for the same 17 elements that were also measured in CS 22874−042. CD −48 2445 shows a slightly higher [α/Fe] = 0.39 ± 0.14, but a similarly low Al and Mn abundance, and a general increased level of the *s*−process elements Sr, Zr, Ba, and La. Interestingly, this hot star has an *r*−process enhancement of [Eu/Fe] = 0.85.

4.3. Uncertainties

To assess the uncertainties due to stellar parameters, we determined the abundances in the same way as in Jofré et al. (2015), using `iSpec`. To wit, we determined the abundances eight times, each one considering a different value of the stellar parameters given their uncertainty. The results for each star are indicated in Table 8. The error due to uncertainty in each of the stellar parameters are given as Δ(Teff), Δ($\log g$), Δ([Fe/H]) and Δ(vmic), respectively.

Table 8. Final uncertainties in the abundances of CS 22874-042. The variation obtained considering the uncertainties in stellar parameters are given under the variable Δ for T, logg, [Fe/H], and ξ, respectively. The last column indicates the number of lines used for each element.

	CS 22874-042				CD −48 2445				
Element	Δ(Teff)	Δ(logg)	Δ([Fe/H])	Δ(ξ)	Δ(Teff)	Δ(logg)	Δ([Fe/H])	Δ(ξ)	N lines
Li	0.131	0.000	0.010	0.015	0.07	0.00	0.00	0.00	1
C	–	–	–	–	0.50	0.13	0.61	0.01	2
O	0.125	0.076	0.009	0.013	–	–	–	–	0
Na	0.171	0.052	0.003	0.005	0.08	0.02	0.00	0.03	2
Mg	0.073	0.003	0.004	0.005	0.04	0.00	0.00	0.00	3
Al	0.123	0.000	0.025	0.043	0.06	0.00	0.01	0.02	2
Si	–	–	–	–	0.08	0.03	0.00	0.03	1
Ca	0.170	0.051	0.005	0.007	0.09	0.03	0.00	0.01	4
Sc	0.094	0.071	0.004	0.006	0.05	0.03	0.00	0.01	3
Ti	0.049	0.074	0.002	0.002	0.03	0.04	0.00	0.00	1
V	0.042	0.074	0.005	0.009	0.02	0.04	0.00	0.00	1
Cr	0.187	0.008	0.007	0.010	0.09	0.00	0.00	0.05	2
Mn	0.186	0.002	0.007	0.010	0.10	0.00	0.00	0.01	3
Co	0.143	0.010	0.010	0.015	0.07	0.00	0.00	0.00	2
Ni	0.146	0.004	0.010	0.015	0.07	0.00	0.00	0.00	1
Sr	0.132	0.044	0.017	0.028	0.07	0.02	0.01	0.08	2
Y	–	–	–	–	0.03	0.05	0.00	0.00	2
Zr	–	–	–	–	0.09	0.00	0.00	0.00	2
Ba	0.112	0.065	0.007	0.012	0.05	0.03	0.00	0.01	1
Eu	–	–	–	–	0.02	0.04	0.00	0.00	1

Table 7. Final elemental abundances measured for CS 2287−042 and CD−48 2445. The uncertainty (σ) covers to the line-to-line scatter and continuum placement.

	CS 22874−042		CD −48 2445	
Elem.	[X/Fe]	σ	[X/Fe]	σ
Li I	2.38	0.10	2.23	-
CH	0.0	0.2	<0.0	-
O I	0.45	0.10	–	–
Na I	0.22	0.05	0.19	
Mg I	0.35	0.10	0.55	0.05
Al I	−0.85	0.05	−0.83	0.09
Si I	0.25	0.10	0.20	0.10
Ca I	0.28	0.10	0.38	0.0
Sc II	0.30	0.05	0.26	0.05
Ti I	0.46	0.15	–	–
Ti II	0.37	0.10	0.42	0.04
V II	0.30	0.10	0.27	0.2
Cr I	0.20	0.05	−0.05	0.05
Mn I	−0.45	0.05	−0.45	0.01
Co I	0.00	0.05	0.11	0.04
Ni I	−0.05	0.05	< 0.10	–
Sr II	0.15	0.10	0.50	0.15
Y II	0.15	0.15	0.05	0.05
Zr II	< 1	–	0.70	0.15
Ba II	0.0	0.10	0.24	0.04
La II	< 0.5	–	0.70	0.10
Eu II	–	–	0.85	0.1

4.3.1. NLTE effects

Our work is based on abundances obtained under the assumption of one-dimensional (1D) model atmospheres and that LTE holds for all species. However, it is known that metal-poor stars, especially those with higher temperatures, can be significantly affected by NLTE and 3D effects, especially when deriving atmospheric parameters using low excitation iron lines (Mashonkina et al. 2011; Bergemann et al. 2012; Hansen et al. 2013). This prompted us to determine a photometric temperature for CS 22874−042 . However, iron abundances need to be derived from the spectrum and can have NLTE corrections. For warm BMP stars (T=6500K) with metallicities around −2 the corrections tend to be less than 0.1 dex (Lind et al. 2013), which is similar to our derived Fe uncertainty (Sect. 4.3).

Since HD84937 has a slightly higher temperature and otherwise similar stellar parameters compared to CS 22874−042. We use the NLTE correction for the former star to estimate an order of magnitude of the NLTE corrections. Starting with the lightest element Li, 3D and NLTE corrections typically amount to around 0.1 dex or less (Dobrovolskas et al. 2014; Sbordone et al. 2010; Lind et al. 2009). The corrections for Li are less than the ∼0.2 dex required to lower the Li amount to the Spite plateau value. Sbordone et al. (2010) investigated differences in NLTE vs. LTE Li abundances using two independent model atoms (Carlsson et al. 1994; Lind et al. 2009). In both cases, stars with temperatures hotter than 6500',K have NLTE abundances that are ∼0.04 dex lower than the LTE abundances. We note that for CD −48 2445 the difference due to NLTE reported in (Meléndez et al. 2010) is 0.08 dex. Regardless of 3D, NLTE corrections both BMP stars will remain above the Spite plateu.

Dobrovolskas et al. (2014) investigated the NLTE and 3D effects on sodium and oxygen in main-sequence stars and concluded that the departures from LTE play a dominant role at the 0.35 dex level for Na and 0.20 dex for oxygen. However, due to the much lower influence of convection in the atmospheres of turn-off stars the abundance corrections are significantly smaller in these stars – 0.02 dex for Na and 0.05 dex for O. In comparison Amarsi et al. (2016) report a combined 3D, NLTE correction for O from the 6300Å forbidden line of −0.1 dex in a 6500 K turn-off star. In another study of the NLTE effects of the Na D lines, which are also used in the present work, Lind et al. (2011) showed that the corrections are significant for turn-off

metal-poor stars, but they slightly decrease towards hotter temperatures.

Andrievsky et al. (2008) determined Al NLTE corrections in metal-poor dwarfs and showed that they can reach up to 0.7 dex for a star with parameters similar to CS 22874−042. This brings our seemingly low abundances much better in line with the approximately Solar [Al/Fe] ratios in the metal-poor halo.

For Mg, Si, Ca, the corrections are very small, on the order of 0.02 dex or less, but at ∼0.25 dex, for Cr the NLTE effects in metal-poor stars are more significant (Bergemann & Cescutti 2010). The need for large NLTE correction for Cr was recently reduced by using improved atomic data for the Cr I and Cr II lines (Sneden et al. 2016).

Manganese NLTE effects can also be significant for metal-poor stars (Bergemann & Gehren 2008). In the recent study of HD 84937 Sneden et al. (2016) discussed the Mn resonance lines $\lambda\lambda$ 4030, 4033, 4034 Å, which have corrections of more than 0.5 dex. For the s-process element Sr, the detailed spectroscopic analysis of Hansen et al. (2013) showed that differences between NLTE and LTE in Sr II abundances (from the 4077 Å-line) in the warmest, metal-poor dwarfs of their sample could reach 0.12 dex. In contrast, the neutral 4607 Å-line experiences a much larger departure from LTE. For Ba, the study of Andrievsky et al. (2009) and Korotin et al. (2015) show that, as for Sr, NLTE will as a function of temperature act differently on different transitions. For instance, the line at 4554 Åused in our study, has NLTE effects on the order of 0.1 dex in BMP stars.

Unfortunately there have been no studies on NLTE corrections spanning the large parameter range of blue stragglers or BMP stars in the literature. As we have seen above, most of the corrections remain minor (within the derived uncertainty) except from an element like Al. Therefore, in the next section, we limit ourselves to comparing the chemical abundances of CS 22874−042 and CD −48 2445 to other warm dwarf stars, which have also been analysed assuming 1D-LTE. Although the chemical abundances might be subject to some corrections, the *relative* comparison between the abundances in stars with similar stellar parameters still sheds light on the nature of BMP stars.

5. Discussion of BMP formation sites

5.1. Correlation with stellar rotation

Boesgaard & Tripicco (1986) noted a strong decline in the Li-abundance within a very narrow temperature window ±300 K in Pop I and old, open cluster stars. Reasons for this comprise differential rotation, meridional circulation, convection and/or diffusion effects, all of which involves transport of the surface Li to deeper, hotter layers, where it is easily destroyed. A trend of Li abundance and rotational properties thus arises naturally. Such a dip has not been seen in young star clusters, while it is more evident in old, metal-poor systems. Dearborn et al. (1992) suggest that mass loss during the main sequence phase can cause the Li-dip, which predicts that a similar depletion should be observed in metal-poor Pop II systems, as indeed first evidenced in Asplund et al. (2006); Bonifacio et al. (2007). Here we do not find evidence of a Li-dip in the range 6400–6800 K since both single stars and binary candidates remain at the Spite Plateau, except from the BMP binaries that are naturally depleted in Li (see Fig. 5).

As a consequence of the well-established relation between rotation and spectral type (e.g., Nielsen et al. 2013), we show in Fig. 6 selected spectral lines in HD 142575 compared to their counterparts in CS 22874−042 and CD −48 2445. HD 142575 is also a BMP star, but it is hotter and rotates faster, as can be seen from the broadened spectral lines. For this star, Carney et al. (2005) list an A(Li) of 1.45 dex and an EW of 2.1 mÅ was reported by Fulbright (2000). Our spectrum of higher SNR and higher resolution did not permit us to measure an EW for this line, which implies that HD 142575 is clearly Li-depleted. Using a sample of halo stars that experienced mass transfer Masseron et al. (2012) showed that all stars with large rotational velocities (> 8 km s^{-1}) had depleted Li, while all stars with normal Li were slow rotators. This is confirmed by our sample, where the fast rotator HD 142575 is depleted in Li, while the stars with lower v sin i (CS 22874−042 and CD −48 2445) have high-to-normal Li. We note that despite the lower v sin i/v$_{macro}$ CD −48 2445 may still have experienced mass transfer (see below).

5.2. s-process and AGB enhancement

We find that CD −48 2445 is s-process enhanced (notably in La, Zr, and Sr) with respect to CS 22874−042. While both stars have a comparable abundance pattern of iron-peak and α−elements, they show a clear difference in their enrichment patterns at a 0.2 dex level or more in the heavy r− and s−elements (see Table 7).

An apparent RV variation of CD −48 2445 (seen over 40 years), and this star falling below the colour cut $V - Ks_0 = 1.08$ would point towards binarity and mass transfer from an AGB star affecting its abundance pattern. Owing to the Ba and especially La enrichment, the AGB polluting CD −48 2445 was likely of a lower mass, since already a 2 M$_\odot$ AGB would produce and transfer much larger abundances than what we detect observationally (Izzard et al. (2009) and Cristallo et al. (2011)). That is, a 1.3 M$_\odot$ AGB or even slightly lower mass would agree better with the observed (low) Ba abundance (see e.g. Cristallo et al. 2011). The enhancement of s− process with respect to CS 22874−042 suggest that the variation of RV is real.

5.3. Origin of BMP stars and comparison with the literature

CS 22874−042 shows evidence of being a regular halo star in many regards, such as its elevated [α/Fe] ratios, which, at its metallicity of −1.9 dex, would argue against an accretion origin from a dwarf galaxy unless the stripped satellite had been massive with a high star formation rate to reach this level of α enhancement (e.g., Hendricks et al. 2014). In either case its abundance pattern points to a scenario where this star has had time to be enriched by several SNe at a [Fe/H]> −2 dex and a mean [α/Fe] of 0.35 dex.

However, at [Fe/H]∼ −2 (after less than 1 Gyr on the enrichment clock), yields from SN Ia have not appeared yet in a standard Galactic chemical evolution scenario, so several SNe II will have had time to explode and enrich the ISM.

To aid our interpretation on the BMP star formation mechanisms, we compare our abundance measurements of CS 22874−042 and CD −48 2445 to three other hot dwarfs from the literature. These are: HD 106038 (this halo star has a very similar enhancement of Li to CS 22874−042; Asplund et al. (2006)); HD 84937 (usually treated as a typical halo star with no signatures of binarity, pollution or extra mixing); and CS 22950−173 (with similar temperatures to our sample but normal Li abundance; Sbordone et al. (2010)).

Here, CS 22950−173 is interesting since it also belongs to the RV constant sample from PS00. Our spectrum for this star was too noisy to detect Li, but the UVES spectrum used by

Table 9. Literature abundance for our comparison stars.

Element	HD 106038		HD 84937		CS 22950-173	
	[X/Fe]	Reference	[X/Fe]	Reference	[X/Fe]	Reference
Li	2.48	A06	2.30	T94	2.20–2.30	S10
Mg	0.36	N97	0.27	J15	0.38	PS00
Al	-		−0.89	M08	-	
Si	0.57	N97	0.30	J15	...	...
Ca	0.21	N97	0.36	J15	0.18	PS00
Sc	0.17	B15	0.13	J15	−0.01	PS00
Ti	0.19	N97	0.37	J15	0.53	PS00
V	...	...	0.25	S16	...	...
Cr	0.02	N97	−0.20	J15	−0.08	PS00
Mn	−0.20	P13	−0.27	S16	< −0.13	PS00
Co	0.10	P13	0.14	S16	...	...
Ni	0.18	N97	0.00	J15	...	...
Sr	0.56	H12	−0.03	M08	−0.74	PS00
Y	0.54	H12	0.00	M08	...	...
Zr	0.68	H12	0.25	M08	...	...
Ba	0.76	H12	−0.15	M08	−0.04	PS00
Eu	0.45	H12	0.54	M08	...	...

Notes. References: A06: Asplund et al. (2006), N97: Nissen & Schuster (1997), B15: Battistini & Bensby (2015), P13: Peterson (2013), H13: Hansen et al. (2013), H12: Hansen et al. (2012), T94: Thorburn (1994), J15: Jofré et al. (2015), S16: Sneden et al. (2016), M07: Mashonkina et al. (2007), F00: Fulbright (2000), M08: Mashonkina et al. (2008), S10: Sbordone et al. (2010), PS00: Preston & Sneden (2000), S14: Spite et al. (2014).

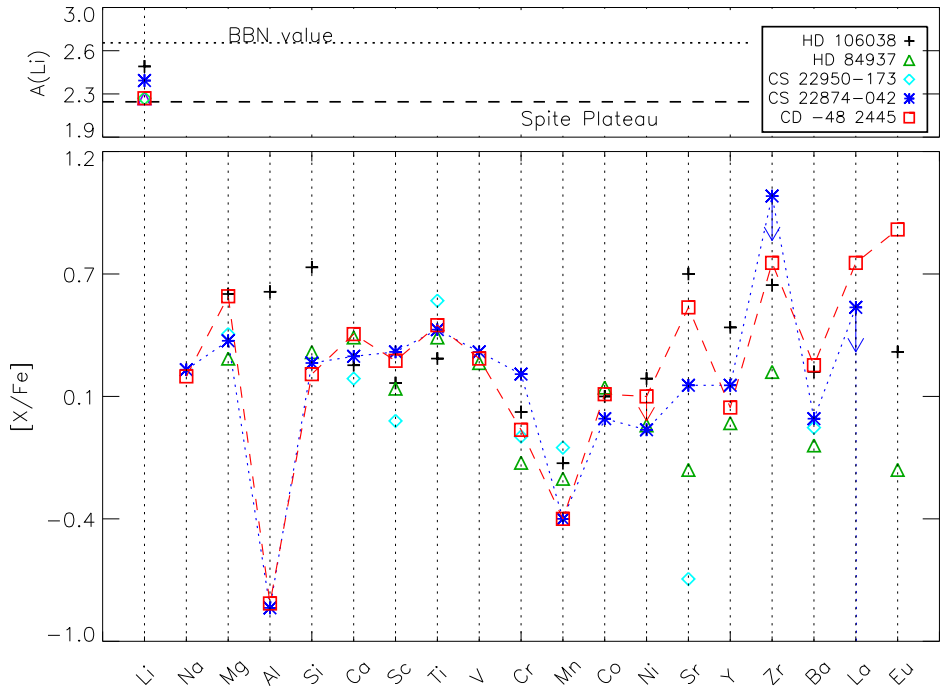

Fig. 7. Abundance pattern for CS 22874−042, CD −48 2445 and our comparison stars HD 106038, HD 84937, and CS 22950-173. The abundances of the comparison stars have been taken from the literature (see Table 9). We also indicate the BBN Li level from WMAP (A(Li)=2.7 Cyburt et al. 2008) as well as the Spite Plateau (2.2).

Sbordone et al. (2010) allowed them to robustly detect Li. Moreover, it is important to note that Sbordone et al. (2010) determined the temperature for this metal-poor dwarf using different methods. With their NLTE calculations for the Balmer lines they obtained a temperature for this BMP star significantly lower (6335 – 6506 K) than in PS00 (6800 K), similar to what we found for CS 22874−042. For our comparison, we employ literature studies preferentially using LTE for the sake of consistency. The respective results from the literature are indicated in Table 9.

As it transpires, all stars have relatively homogeneous values in the $\alpha-$ and iron-peak element abundances. Their scatter can be attributed to differences in, e.g., different techniques for the abundance determination between the sources and differences in stellar parameters. This can induce a scatter in the

abundances of more than 0.2 dex, especially for those elements that are affected by hyperfine structure, such as the odd-Z iron-peak elements (Smiljanic et al. 2014; Jofré et al. 2015). Other abundance peculiarities, such as the strong Si- and *s*-process enhancement in HD 106038 remain hard to explain to date, even more so given the RV-constancy (Nissen & Schuster 1997) and our colour method supports that this star is single, since it is located above the $V - Ks_0 = 1.08$ cut.

It is interesting to note that the neutron-capture elements differ by more than 0.2 dex and as such the difference are unlikely to be attributed to different measurement techniques as above (cf. Table 8). In Galactic chemical evolution this is expected, where abundances of these elements present a scatter of up to one dex at these metallicities (Sneden et al. 2008; Hansen et al. 2012, 2014). In this regard, HD 106038 is interesting in that it is systematically enhanced in all neutron-capture elements with respect to the other stars. Smiljanic et al. (2008) suggested that a hypernova could have caused the enrichment seen in Be and Li, however, they had problems explaining the observed ^{6}Li as well as other elemental abundances. As this star has a metallicity of −1.48 both supernovae (SN) and AGB stars can easily have contributed to the gas mixture that created this star. We therefore suggest that the observationally derived abundances are a result of AGB plus either magneto-hydrodynamic (MHD) SN (Winteler et al. 2012) or neutron star mergers (NSM) which could explain the enhanced levels of the neutron-capture elements. This agrees well with a [Ba/Eu][4] = 0.31 pointing towards a mixed *r*− and *s*−process origin (Hansen et al. (2012); Mashonkina et al. (2008), and Arlandini et al. (1999); Bisterzo et al. (2014)).

In HD 84937 a very different chemical pattern is seen for the heavy elements (see Table 9 and Fig. 7). Here the [Ba/Eu]∼ −0.7 indicates an almost pure r-process enrichment at a lower metallicity (−2.15 Mashonkina et al. 2008). This would indicate a large contribution from either MHD SN or NSM.

The last star taken from the literature is CS 22950−173 which is underabundant in the two known heavy elements Sr and Ba. Based on the low levels, a possible formation site could be the fast rotating massive stars (Frischknecht et al. 2012), however, the reverse abundance ratios would be expected for Sr and Ba (i.e., Sr>Ba). According to Arlandini et al. 1999 and Mashonkina et al. (2008) a [Sr/Ba]<0.62 could also indicate an *r*−process origin, which in this star would be very diluted (or inefficient thereby making 'normal' SN an option).

Although CS 22874−042 and CD −48 2445 have very similar iron-peak and α−abundances, the abundances of *s*−process elements differ. We therefore believe that CD −48 2445 is a result of AGB yields mixed with an efficient *r*−site like NSM or MHD SN, while CS 22874−042 is more likely enriched by massive rotating stars or normal (massive) supernovae creating the high level of α−elements and the low level of neutron-capture elements. We note that the low Ba abundance is a bit puzzling, and while the Ba/Eu-ratio would indicate a very r-process dominated gas origin of CD −48 2445 the La/Eu-ratio would point towards a more convolved *r*− and *s*−process mixture, which we support based on the high level of Sr and Zr in this star.

6. Summary and Conclusions

In the era of large surveys we are bound to observe blue metal-poor stars in large numbers as they are often bright. Thus, it is becoming increasingly important to understand their origin in order to explore their potential as chemical tracers and segregators of galaxy formation scenarios.

Blue metal-poor stars are important probes of Galactic evolution because they are either younger than typical turn-off stars of the halo, or because they are field blue stragglers (binaries). Here we developed a way, which to first order relies on colour and photometry, to separate the binaries from the single stars, immediately allowing the blue stragglers to be singled out amongst the blue stars. We find a cut at $V - Ks_0 = 1.08$ mag below which the binaries fall in 97% of the cases (including some single star pollution possibly caused by fast rotating stars). Above this cut (almost only) single stars are found. The method is further improved by combining photometry and spectroscopy (comparing the $V - Ks_0$ to the stellar Li abundance, a useful indicator as mentioned by Carney et al. (2005)). However, this second step requires high-resolution, high SNR spectra. Spectral analysis of these objects is thus a vital tool for disentangling details about their origin as well as chemical tagging of their composition and assessment of birthplace and nuclear formation processes. Further information can be drawn from mass-transfer signatures (e.g., *s*−process elements) that might have affected their evolution. These analyses are, however, challenging, as their hot and metal-poor nature makes the identification of spectral lines difficult, and large telescopes are needed to obtain a spectrum with high enough SNR. Moreover, repeat observations covering an extended timespan of several years are needed to assess binarity based on RV measurements in such stars. For this reason, there is little information about their chemical composition available in the literature. Here we contributed to this field with a new way of separating binary from single blue stars combined detailed chemical analysis of two BMP stars in a comparison with similar stars from the literature. Our results can be summarised as following:

- *Colour separation of binary and single stars:* Here we used $V - Ks_0$ vs $B - V_0$ or metallicity to separate blue binary stars from single stars. A colour cut at $V - Ks_0 = 1.08$ mag was discovered. This is useful in surveys (such as Gaia) that provide colour and metallicity. Moreover, we show how Li abundances combined with photometry allow for a smooth and fast separation of which BMP stars are binaries and which are single stars.
- *Stellar parameters:* With our improved high-quality spectrum and a new parameter determination, we found a significantly lower temperature of CS 22874−042 than had originally been determined in PS00. Such discrepancies have also been reported in the literature (Sbordone et al. 2010). Since our new effective temperature lowered the Li abundance by almost one dex, this emphasizes the need for accurate and precise stellar parameters when assessing the chemical nature of this class of stars.
- *The behaviour of Li in blue stragglers*: It has been suggested that BMP stars with a regular plateau value of A(Li) should be intermediate-age stars, while Li-depleted stars are more likely to be blue stragglers. Our work showed that this distinction is not that straightforward. One decisive factor is stellar mass, as several theoretical and observational studies have ascertained that the depletion from the primordial BBN value acts more efficiently in lower-mass stars through mass-dependent diffusion (e.g. Richard et al. 2005; González Hernández et al. 2008; Meléndez et al. 2010; Aoki et al. 2012). Similarly, if

[4] [Ba/Eu]< −0.77 indicates a pure *r*−process origin.

mass transfer occurred in these systems, diffusion can be inhibited such that Li could retain its original (high) levels. This is bolstered by our finding of the Li-plateau value in CD −48 2445 which shows other signs of mass transfer; the fact that the Li-enhanced star in our study, CS 22874−042 is clearly a single star, gives weight to our proposed separation. See also Jofre et al. (2016) for discussion on possible Li enhancement in evolved blue stragglers that are not in binary systems.

– *Lithium and rotation in RV constant stars:* HD 142575 is found to be Li depleted and a fast rotating star. CS 22874−042 on the other hand is slowly rotating and Li-enriched confirming that there is a correlation between the rotation and the Li abundance. This agrees with the results of Masseron et al. (2012).
– *RV constancy of CS 22874−042 over 22 years*: Our new RV determination 15 years after the last RV measurement of PS00 confirms that CS 22874−042 does not have a companion that we can detect neither in RV nor in colour.
– *Origin of BMP stars*: From its abundances of $r-$ and $s-$process elements, we conclude that CD −48 2445 might have received prenatal gas from a NSM and is a possible blue straggler that accreted mass from an AGB. It may still have a binary companion in the form of a white dwarf. CS 22874−042 on the other hand has experienced a very different enrichment, possibly from massive stars with inefficient heavy element production. Both stars have a relatively high α-to-Fe ratio making them in situ formed Milky Way stars.

More high SNR spectra and accurate photometry for BMP stars are needed to revise their stellar parameters, determine elemental abundances, and gain extra RV measurement that will give us more insights into how various subgroups of these blue stars are created. Additionally, the photometry will help confirm and generalise the colour cut discovered. The Li, α, $r-$ and $s-$element abundances allow us to distinguish the BMP fraction that are binaries and suffered from mass transfer from the ones that are accreted early on in a galaxy merger event. Hence abundance studies of these elements in such stars will help enlightning us on galaxy formation and evolution and this has an important outlook for the future large surveys that are efficient in the red-wavelenght range (e.g., 4MOST, HIRES, WEAVE).

Acknowledgements. We thank the anonymous referee for helpful and constructive input and G. W. Preston for fruitful discussions. CJH thanks R. Izzard for a useful discussion and acknowledges support from the research grant VKR023371 by the VILLUM FOUNDATION. PJ dedicates this work to J. Jofré, as this analysis was not only motivated to study lithium in BMP stars, but also to find peace in a difficult moment of severe illness. This work has been partially supported by ERC grant number 320360. PJ also acknowledges T. Masseron and C. Tout for useful discussions on this subject, as well as King's College Cambridge for partially supporting this research.

References

Alonso, A., Arribas, S., & Martinez-Roger, C. 1996, A&A, 313, 873
Amarsi, A. M., Asplund, M., Collet, R., & Leenaarts, J. 2016, MNRAS, 455, 3735
Andrievsky, S. M., Spite, M., Korotin, S. A., et al. 2008, A&A, 481, 481
Andrievsky, S. M., Spite, M., Korotin, S. A., et al. 2009, A&A, 494, 1083
Aoki, W., Ito, H., & Tajitsu, A. 2012, ApJ, 751, L6
Arlandini, C., Käppeler, F., Wisshak, K., et al. 1999, ApJ, 525, 886
Armandroff, T. E. & Zinn, R. 1988, AJ, 96, 92
Ashwell, J. F., Jeffries, R. D., Smalley, B., et al. 2005, MNRAS, 363, L81
Asplund, M., Lambert, D. L., Nissen, P. E., Primas, F., & Smith, V. V. 2006, ApJ, 644, 229
Augensen, H. J. 1979, AJ, 84, 1553
Barklem, P. S. 2007, A&A, 466, 327
Battistini, C. & Bensby, T. 2015, A&A, 577, A9
Beers, T. C., Almeida, T., Rossi, S., Wilhelm, R., & Marsteller, B. 2007, ApJS, 168, 277
Bergemann, M. & Cescutti, G. 2010, A&A, 522, A9
Bergemann, M. & Gehren, T. 2008, A&A, 492, 823
Bergemann, M., Lind, K., Collet, R., Magic, Z., & Asplund, M. 2012, MNRAS, 427, 27
Bisterzo, S., Travaglio, C., Gallino, R., Wiescher, M., & Käppeler, F. 2014, ApJ, 787, 10
Blanco-Cuaresma, S., Soubiran, C., Heiter, U., & Jofré, P. 2014a, A&A, 569, A111
Blanco-Cuaresma, S., Soubiran, C., Jofré, P., & Heiter, U. 2014b, A&A, 566, A98
Boesgaard, A. M. & Tripicco, M. J. 1986, ApJ, 302, L49
Bonifacio, P., Molaro, P., Sivarani, T., et al. 2007, A&A, 462, 851
Carlsson, M., Rutten, R. J., Bruls, J. H. M. J., & Shchukina, N. G. 1994, A&A, 288, 860
Carney, B. W., Latham, D. W., & Laird, J. B. 2005, AJ, 129, 466
Casagrande, L., Ramírez, I., Meléndez, J., Bessell, M., & Asplund, M. 2010, A&A, 512, A54
Cristallo, S., Piersanti, L., Straniero, O., et al. 2011, ApJS, 197, 17
Cyburt, R. H., Fields, B. D., & Olive, K. A. 2008, J. Cosmology Astropart. Phys., 11, 012
Dearborn, D. S. P., Schramm, D. N., & Hobbs, L. M. 1992, ApJ, 394, L61
Deliyannis, C. P., Steinhauer, A., & Jeffries, R. D. 2002, ApJ, 577, L39
Dobrovolskas, V., Kučinskas, A., Bonifacio, P., et al. 2014, A&A, 565, A121
Frischknecht, U., Hirschi, R., & Thielemann, F.-K. 2012, A&A, 538, L2
Fulbright, J. P. 2000, AJ, 120, 1841
Gallagher, A. J., Ryan, S. G., Hosford, A., et al. 2012, A&A, 538, A118
González Hernández, J. I., Bonifacio, P., Ludwig, H.-G., et al. 2008, A&A, 480, 233
Hansen, C. J., Bergemann, M., Cescutti, G., et al. 2013, A&A, 551, A57
Hansen, C. J., Montes, F., & Arcones, A. 2014, ApJ, 797, 123
Hansen, C. J., Primas, F., Hartman, H., et al. 2012, A&A, 545, A31
Hansen, C. J., Rich, R. M., Koch, A., et al. 2016, A&A, 590, A39
Heiter, U., Jofré, P., Gustafsson, B., et al. 2015a, A&A, 582, A49
Heiter, U., Lind, K., Asplund, M., et al. 2015b, Phys. Scr, 90, 054010
Hendricks, B., Koch, A., Lanfranchi, G. A., et al. 2014, ApJ, 785, 102
Izzard, R. G., Glebbeek, E., Stancliffe, R. J., & Pols, O. R. 2009, A&A, 508, 1359
Jofré, P., Heiter, U., Soubiran, C., et al. 2015, A&A, 582, A81
Jofré, P., Heiter, U., Soubiran, C., et al. 2014, A&A, 564, A133
Jofre, P., Masseron, T., Izzard, R. G., et al. 2016, ArXiv e-prints
Jofré, P. & Weiss, A. 2011, A&A, 533, A59
Kelson, D. D. 2003, PASP, 115, 688
Koch, A., Lind, K., & Rich, R. M. 2011, ApJ, 738, L29
Korotin, S. A., Andrievsky, S. M., Hansen, C. J., et al. 2015, A&A, 581, A70
Kupka, F., Dubernet, M.-L., & VAMDC Collaboration. 2011, Baltic Astronomy, 20, 503
Lawler, J. E., Bonvallet, G., & Sneden, C. 2001a, ApJ, 556, 452
Lawler, J. E., Wickliffe, M. E., den Hartog, E. A., & Sneden, C. 2001b, ApJ, 563, 1075
Lind, K., Asplund, M., & Barklem, P. S. 2009, A&A, 503, 541
Lind, K., Asplund, M., Barklem, P. S., & Belyaev, A. K. 2011, A&A, 528, A103
Lind, K., Melendez, J., Asplund, M., Collet, R., & Magic, Z. 2013, A&A, 554, A96
Lucatello, S., Tsangarides, S., Beers, T. C., et al. 2005, ApJ, 625, 825
Mashonkina, L., Gehren, T., Shi, J.-R., Korn, A. J., & Grupp, F. 2011, A&A, 528, A87
Mashonkina, L., Zhao, G., Gehren, T., et al. 2008, A&A, 478, 529
Mashonkina, L. I., Vinogradova, A. B., Ptitsyn, D. A., Khokhlova, V. S., & Chernetsova, T. A. 2007, Astronomy Reports, 51, 903
Masseron, T., Johnson, J. A., Lucatello, S., et al. 2012, ApJ, 751, 14
Meléndez, J., Casagrande, L., Ramírez, I., Asplund, M., & Schuster, W. J. 2010, A&A, 515, L3
Monaco, L., Villanova, S., Bonifacio, P., et al. 2012, A&A, 539, A157
Nielsen, M. B., Gizon, L., Schunker, H., & Karoff, C. 2013, A&A, 557, L10
Nissen, P. E. & Schuster, W. J. 1997, A&A, 326, 751
Nissen, P. E. & Schuster, W. J. 2010, A&A, 511, L10
Peterson, R. C. 2013, ApJ, 768, L13
Preston, G. W. 2015, Field Blue Stragglers and Related Mass Transfer Issues, ed. H. M. J. Boffin, G. Carraro, & G. Beccari, 65
Preston, G. W., Shectman, S. A., & Beers, T. C. 1991, ApJS, 76, 1001
Preston, G. W. & Sneden, C. 2000, AJ, 120, 1014
Ramírez, I. & Meléndez, J. 2005, ApJ, 626, 446
Richard, O., Michaud, G., & Richer, J. 2005, ApJ, 619, 538
Ryan, S. G., Beers, T. C., Kajino, T., & Rosolankova, K. 2001, ApJ, 547, 231

Ryan, S. G. & Norris, J. E. 1991, AJ, 101, 1835
Ryan, S. G., Norris, J. E., & Beers, T. C. 1999, ApJ, 523, 654
Sbordone, L., Bonifacio, P., Caffau, E., et al. 2010, A&A, 522, A26
Schlafly, E. F. & Finkbeiner, D. P. 2011, ApJ, 737, 103
Schlegel, D. J., Finkbeiner, D. P., & Davis, M. 1998, ApJ, 500, 525
Sivarani, T., Bonifacio, P., Molaro, P., et al. 2004, A&A, 413, 1073
Skrutskie, M. F., Cutri, R. M., Stiening, R., et al. 2006, AJ, 131, 1163
Smiljanic, R., Korn, A. J., Bergemann, M., et al. 2014, A&A, 570, A122
Smiljanic, R., Pasquini, L., Primas, F., et al. 2008, MNRAS, 385, L93
Sneden, C., Cowan, J. J., & Gallino, R. 2008, ARA&A, 46, 241
Sneden, C., Cowan, J. J., Kobayashi, C., et al. 2016, ApJ, 817, 53
Sneden, C., Lucatello, S., Ram, R. S., Brooke, J. S. A., & Bernath, P. 2014, ApJS, 214, 26
Sneden, C., Preston, G. W., & Cowan, J. J. 2003, ApJ, 592, 504
Sneden, C. A. 1973, PhD thesis, THE UNIVERSITY OF TEXAS AT AUSTIN.
Sobeck, J. S., Lawler, J. E., & Sneden, C. 2007, ApJ, 667, 1267
Spite, F. & Spite, M. 1982, A&A, 115, 357
Spite, M., Spite, F., Bonifacio, P., et al. 2014, A&A, 571, A40
Thorburn, J. A. 1994, ApJ, 421, 318
Unavane, M., Wyse, R. F. G., & Gilmore, G. 1996, MNRAS, 278, 727
Ventura, P. & D'Antona, F. 2011, MNRAS, 410, 2760
Wiese, W. L., Fuhr, J. R., & Deters, T. M. 1996, Atomic transition probabilities of carbon, nitrogen, and oxygen : a critical data compilation
Winteler, C., Käppeli, R., Perego, A., et al. 2012, ApJ, 750, L22
Woosley, S. E. & Weaver, T. A. 1995, ApJS, 101, 181
Yan, Z.-C., Tambasco, M., & Drake, G. W. F. 1998, Phys. Rev. A, 57, 1652

Appendix A: Line list

Table A.1. Line list used in our analysis. References correspond to WIE: Wiese et al. (1996); SNE: Sneden et al. (2014); LAW: Lawler et al. (2001a,b); SOB: Sobeck et al. (2007); YAN: Yan et al. (1998); GAL: Gallagher et al. (2012).

Wavelength [Å]	Species	log gf	E.P. [eV]	Reference
Li				
6707.764	3.0	-0.002	0.000	YAN
6707.915	3.0	-0.303	0.000	YAN
6707.921	3.0	-0.002	0.000	YAN
6708.072	3.0	-0.303	0.000	YAN
O				
7771.940	8.0	0.370	9.140	WIE
7774.170	8.0	0.220	9.140	WIE
7775.390	8.0	0.000	9.140	WIE
Na				
5889.951	11.0	0.117	0.000	SNE
5895.924	11.0	-0.184	0.000	SNE
Mg				
4057.505	12.0	-1.201	4.343	SNE
4167.271	12.0	-1.004	4.343	SNE
4702.991	12.0	-0.666	4.343	SNE
5528.405	12.0	-0.620	4.343	SNE
Al				
3944.006	13.0	-0.623	0.000	SNE
3961.520	13.0	-0.323	0.014	SNE
Si				
3905.523	14.0	-1.090	1.907	SNE
7405.772	14.0	-0.820	5.609	SNE
7415.948	14.0	-0.500	5.611	SNE
Ca				
4226.728	20.0	0.243	0.000	SNE
4283.011	20.0	-0.224	1.884	SNE
4289.367	20.0	-0.303	1.878	SNE
4298.988	20.0	-0.412	1.884	SNE
4302.528	20.0	0.275	1.897	SNE
4307.744	20.0	-0.256	1.884	SNE
4318.652	20.0	-0.208	1.897	SNE
4425.437	20.0	-0.385	1.878	SNE
4434.957	20.0	-0.029	1.884	SNE
4435.679	20.0	-0.500	1.884	SNE
4454.779	20.0	0.252	1.897	SNE
4455.887	20.0	-0.510	1.897	SNE
4585.865	20.0	-0.186	2.524	SNE
5264.237	20.0	-0.720	2.521	SNE
5265.556	20.0	-0.260	2.521	SNE
5588.749	20.0	0.210	2.524	SNE
5594.462	20.0	-0.050	2.521	SNE
5598.480	20.0	-0.220	2.519	SNE
5601.277	20.0	-0.690	2.524	SNE
5857.451	20.0	0.230	2.930	SNE
6102.723	20.0	-0.890	1.878	SNE
6122.217	20.0	-0.409	1.884	SNE
6162.173	20.0	0.100	1.897	SNE
6439.075	20.0	0.470	2.524	SNE
6462.567	20.0	0.310	2.521	SNE
6493.781	20.0	0.140	2.519	SNE
Sc				
4246.813	21.1	-0.385	0.315	LAW
4246.813	21.1	-0.955	0.315	LAW
4246.820	21.1	-0.783	0.315	LAW
4246.820	21.1	-0.797	0.315	LAW
4246.820	21.1	-0.955	0.315	LAW
4246.826	21.1	-0.797	0.315	LAW
4246.826	21.1	-0.808	0.315	LAW
4246.826	21.1	-1.479	0.315	LAW
4246.831	21.1	-0.808	0.315	LAW

Table A.1 – *Continued*

Wavelength [Å]	Species	log gf	E.P. [eV]	Reference
4246.831	21.1	-0.981	0.315	LAW
4246.831	21.1	-2.905	0.315	LAW
4246.834	21.1	-0.981	0.315	LAW
4246.834	21.1	-1.157	0.315	LAW
4314.076	21.1	-2.782	0.618	LAW
4314.078	21.1	-1.569	0.618	LAW
4314.079	21.1	-2.379	0.618	LAW
4314.080	21.1	-0.640	0.618	LAW
4314.081	21.1	-1.364	0.618	LAW
4314.082	21.1	-0.761	0.618	LAW
4314.082	21.1	-2.167	0.618	LAW
4314.083	21.1	-1.298	0.618	LAW
4314.083	21.1	-2.057	0.618	LAW
4314.084	21.1	-0.897	0.618	LAW
4314.084	21.1	-1.302	0.618	LAW
4314.085	21.1	-1.053	0.618	LAW
4314.085	21.1	-2.036	0.618	LAW
4314.086	21.1	-1.238	0.618	LAW
4314.086	21.1	-1.363	0.618	LAW
4314.086	21.1	-1.485	0.618	LAW
4314.086	21.1	-2.145	0.618	LAW
4314.087	21.1	-1.472	0.618	LAW
4314.087	21.1	-1.668	0.618	LAW
4314.087	21.1	-1.814	0.618	LAW
4320.725	21.1	-2.448	0.605	LAW
4320.727	21.1	-2.030	0.605	LAW
4320.728	21.1	-1.650	0.605	LAW
4320.728	21.1	-1.796	0.605	LAW
4320.729	21.1	-1.448	0.605	LAW
4320.729	21.1	-1.553	0.605	LAW
4320.730	21.1	-1.232	0.605	LAW
4320.730	21.1	-1.265	0.605	LAW
4320.730	21.1	-1.291	0.605	LAW
4320.730	21.1	-1.474	0.605	LAW
4320.732	21.1	-1.775	0.605	LAW
4320.733	21.1	-1.086	0.605	LAW
4320.733	21.1	-1.357	0.605	LAW
4320.734	21.1	-0.708	0.605	LAW
4320.734	21.1	-0.879	0.605	LAW
4324.984	21.1	-1.931	0.595	LAW
4324.986	21.1	-1.491	0.595	LAW
4324.988	21.1	-1.220	0.595	LAW
4324.992	21.1	-1.116	0.595	LAW
4324.992	21.1	-1.232	0.595	LAW
4324.993	21.1	-1.236	0.595	LAW
4324.999	21.1	-1.491	0.595	LAW
4325.000	21.1	-1.036	0.595	LAW
4325.002	21.1	-0.743	0.595	LAW
4400.379	21.1	-2.010	0.605	LAW
4400.383	21.1	-1.202	0.605	LAW
4400.383	21.1	-1.815	0.605	LAW
4400.387	21.1	-1.430	0.605	LAW
4400.387	21.1	-1.762	0.605	LAW
4400.390	21.1	-1.716	0.605	LAW
4400.390	21.1	-1.788	0.605	LAW
4400.392	21.1	-2.010	0.605	LAW
4400.393	21.1	-1.887	0.605	LAW
4400.393	21.1	-2.102	0.605	LAW
4400.394	21.1	-1.815	0.605	LAW
4400.395	21.1	-2.732	0.605	LAW
4400.396	21.1	-1.762	0.605	LAW
4400.396	21.1	-2.109	0.605	LAW
4400.398	21.1	-1.788	0.605	LAW
4400.398	21.1	-1.887	0.605	LAW
4400.398	21.1	-2.586	0.605	LAW
4400.399	21.1	-2.109	0.605	LAW
4415.543	21.1	-1.864	0.595	LAW
4415.548	21.1	-1.706	0.595	LAW

Table A.1 – *Continued*

Wavelength [Å]	Species	log gf	E.P. [eV]	Reference
4415.552	21.1	-1.717	0.595	LAW
4415.554	21.1	-1.294	0.595	LAW
4415.556	21.1	-1.692	0.595	LAW
4415.556	21.1	-1.890	0.595	LAW
4415.559	21.1	-2.388	0.595	LAW
4415.560	21.1	-3.814	0.595	LAW
4415.562	21.1	-2.066	0.595	LAW
4415.567	21.1	-1.706	0.595	LAW
4415.567	21.1	-1.717	0.595	LAW
4415.567	21.1	-1.864	0.595	LAW
4415.567	21.1	-1.890	0.595	LAW
Ti				
3491.049	22.1	-1.100	0.112	LAW
3504.891	22.1	0.380	1.890	LAW
3535.407	22.1	0.010	2.060	LAW
3596.047	22.1	-1.070	0.607	LAW
3659.761	22.1	-0.540	1.581	LAW
3662.232	22.1	-0.540	1.565	LAW
3741.638	22.1	-0.070	1.581	LAW
3761.321	22.1	0.180	0.573	LAW
3813.388	22.1	-1.890	0.607	LAW
3814.580	22.1	-1.680	0.573	LAW
3913.461	22.1	-0.360	1.115	LAW
3948.671	22.0	-0.400	0.000	LAW
3981.762	22.0	-0.270	0.000	LAW
3989.758	22.0	-0.130	0.021	LAW
3998.636	22.0	0.020	0.048	LAW
4012.384	22.1	-1.780	0.573	LAW
4025.129	22.1	-2.110	0.607	LAW
4028.338	22.1	-0.920	1.890	LAW
4053.821	22.1	-1.070	1.891	LAW
4161.529	22.1	-2.090	1.083	LAW
4163.644	22.1	-0.130	2.588	LAW
4171.904	22.1	-0.300	2.596	LAW
4173.533	22.1	-1.880	1.083	LAW
4290.215	22.1	-0.870	1.164	LAW
4300.042	22.1	-0.460	1.179	LAW
4301.923	22.1	-1.210	1.160	LAW
4305.907	22.0	0.490	0.848	LAW
4312.860	22.1	-1.120	1.179	LAW
4394.059	22.1	-1.770	1.220	LAW
4395.031	22.1	-0.540	1.083	LAW
4395.839	22.1	-1.930	1.242	LAW
4399.765	22.1	-1.200	1.236	LAW
4417.719	22.1	-1.430	1.164	SNE
4443.801	22.1	-0.710	1.079	LAW
4450.482	22.1	-1.520	1.083	LAW
4468.493	22.1	-0.630	1.130	LAW
4501.270	22.1	-0.770	1.115	LAW
4529.480	22.1	-1.750	1.571	LAW
4533.239	22.0	0.540	0.848	LAW
4534.776	22.0	0.350	0.835	LAW
4549.622	22.1	-0.220	1.583	LAW
4563.761	22.1	-0.960	1.220	SNE
4571.971	22.1	-0.310	1.571	LAW
4805.085	22.1	-1.100	2.060	SNE
4981.731	22.0	0.570	0.848	LAW
5007.209	22.0	0.170	0.818	LAW
5129.156	22.1	-1.340	1.890	LAW
5226.543	22.1	-1.300	1.565	SNE
V				
4005.706	23.1	-0.460	1.816	SNE
Cr				
3919.150	24.0	-0.710	1.029	SOB
4254.330	24.0	-0.090	0.000	SOB
4274.800	24.0	-0.220	0.000	SOB
4289.720	24.0	-0.370	0.000	SOB
5206.040	24.0	0.020	0.941	SOB

Table A.1 – *Continued*

Wavelength [Å]	Species	log gf	E.P. [eV]	Reference
5208.420	24.0	0.170	0.941	SOB
Mn				
4030.492	25.0	-5.078	3.071	KUR
4030.495	25.0	-4.756	3.071	KUR
4030.500	25.0	-4.932	3.071	KUR
4030.511	25.0	-5.124	3.071	KUR
4030.516	25.0	-4.601	3.071	KUR
4030.524	25.0	-4.522	3.071	KUR
4030.540	25.0	-5.300	3.071	KUR
4030.548	25.0	-4.580	3.071	KUR
4030.558	25.0	-4.249	3.071	KUR
4030.580	25.0	-5.680	3.071	KUR
4030.590	25.0	-4.726	3.071	KUR
4030.602	25.0	-4.037	3.071	KUR
4030.730	25.0	-1.064	0.000	LAW
4030.744	25.0	-1.982	0.000	LAW
4030.746	25.0	-1.204	0.000	LAW
4030.756	25.0	-3.200	0.000	LAW
4030.758	25.0	-1.806	0.000	LAW
4030.759	25.0	-1.362	0.000	LAW
4030.767	25.0	-2.848	0.000	LAW
4030.769	25.0	-1.780	0.000	LAW
4030.770	25.0	-1.546	0.000	LAW
4030.775	25.0	-2.722	0.000	LAW
4030.777	25.0	-1.847	0.000	LAW
4030.777	25.0	-1.768	0.000	LAW
4030.781	25.0	-2.802	0.000	LAW
4030.782	25.0	-2.023	0.000	LAW
4030.782	25.0	-2.053	0.000	LAW
4033.044	25.0	-1.229	0.000	LAW
4033.046	25.0	-2.007	0.000	LAW
4033.056	25.0	-2.007	0.000	LAW
4033.058	25.0	-1.492	0.000	LAW
4033.060	25.0	-1.844	0.000	LAW
4033.068	25.0	-1.844	0.000	LAW
4033.070	25.0	-1.823	0.000	LAW
4033.071	25.0	-1.839	0.000	LAW
4033.078	25.0	-1.839	0.000	LAW
4033.079	25.0	-2.270	0.000	LAW
4033.080	25.0	-1.941	0.000	LAW
4033.084	25.0	-1.941	0.000	LAW
4033.085	25.0	-2.969	0.000	LAW
4033.085	25.0	-2.203	0.000	LAW
4033.088	25.0	-2.203	0.000	LAW
4033.178	25.0	-2.952	3.133	KUR
4033.178	25.0	-3.596	3.133	KUR
4033.184	25.0	-2.898	3.133	KUR
4033.184	25.0	-3.399	3.133	KUR
4033.184	25.0	-3.596	3.133	KUR
4033.193	25.0	-2.792	3.133	KUR
4033.193	25.0	-3.343	3.133	KUR
4033.193	25.0	-3.399	3.133	KUR
4033.203	25.0	-2.668	3.133	KUR
4033.203	25.0	-3.343	3.133	KUR
4033.203	25.0	-3.384	3.133	KUR
4033.216	25.0	-2.540	3.133	KUR
4033.216	25.0	-3.384	3.133	KUR
4033.216	25.0	-3.574	3.133	KUR
4033.231	25.0	-2.415	3.133	KUR
4033.231	25.0	-3.574	3.133	KUR
4034.338	25.0	-4.894	3.133	KUR
4034.338	25.0	-5.405	3.133	KUR
4034.338	25.0	-6.502	3.133	KUR
4034.345	25.0	-4.761	3.133	KUR
4034.345	25.0	-5.217	3.133	KUR
4034.345	25.0	-6.371	3.133	KUR
4034.353	25.0	-4.631	3.133	KUR
4034.353	25.0	-5.162	3.133	KUR

Table A.1 – *Continued*

Wavelength [Å]	Species	log *gf*	E.P. [eV]	Reference
4034.353	25.0	-6.468	3.133	KUR
4034.364	25.0	-4.509	3.133	KUR
4034.364	25.0	-5.200	3.133	KUR
4034.364	25.0	-6.803	3.133	KUR
4034.377	25.0	-4.396	3.133	KUR
4034.377	25.0	-5.388	3.133	KUR
4034.392	25.0	-4.292	3.133	KUR
4034.469	25.0	-1.358	0.000	LAW
4034.471	25.0	-2.047	0.000	LAW
4034.472	25.0	-3.002	0.000	LAW
4034.483	25.0	-1.570	0.000	LAW
4034.485	25.0	-1.901	0.000	LAW
4034.486	25.0	-2.621	0.000	LAW
4034.494	25.0	-1.843	0.000	LAW
4034.495	25.0	-1.922	0.000	LAW
4034.496	25.0	-2.445	0.000	LAW
4034.501	25.0	-2.253	0.000	LAW
4034.502	25.0	-2.077	0.000	LAW
4034.503	25.0	-2.399	0.000	LAW
4034.717	25.0	-3.312	3.133	KUR
4034.717	25.0	-3.567	3.133	KUR
4034.722	25.0	-3.248	3.133	KUR
4034.722	25.0	-3.369	3.133	KUR
4034.722	25.0	-3.567	3.133	KUR
4034.729	25.0	-3.073	3.133	KUR
4034.729	25.0	-3.304	3.133	KUR
4034.729	25.0	-3.369	3.133	KUR
4034.738	25.0	-2.881	3.133	KUR
4034.738	25.0	-3.304	3.133	KUR
4034.738	25.0	-3.335	3.133	KUR
4034.750	25.0	-2.696	3.133	KUR
4034.750	25.0	-3.335	3.133	KUR
4034.750	25.0	-3.517	3.133	KUR
4034.765	25.0	-2.525	3.133	KUR
4034.765	25.0	-3.517	3.133	KUR
Co				
3872.945	27.0	-2.183	3.512	KUR
3872.945	27.0	-2.379	3.512	KUR
3872.953	27.0	-2.158	3.512	KUR
3872.953	27.0	-2.169	3.512	KUR
3872.953	27.0	-2.379	3.512	KUR
3872.965	27.0	-2.031	3.512	KUR
3872.965	27.0	-2.055	3.512	KUR
3872.965	27.0	-2.158	3.512	KUR
3872.981	27.0	-1.864	3.512	KUR
3872.981	27.0	-2.012	3.512	KUR
3872.981	27.0	-2.055	3.512	KUR
3873.001	27.0	-1.695	3.512	KUR
3873.001	27.0	-2.012	3.512	KUR
3873.001	27.0	-2.023	3.512	KUR
3873.026	27.0	-1.536	3.512	KUR
3873.026	27.0	-2.023	3.512	KUR
3873.026	27.0	-2.100	3.512	KUR
3873.054	27.0	-1.388	3.512	KUR
3873.054	27.0	-2.100	3.512	KUR
3873.054	27.0	-2.315	3.512	KUR
3873.086	27.0	-1.252	3.512	KUR
3873.086	27.0	-2.315	3.512	KUR
3873.006	27.0	-4.220	2.278	KUR
3873.006	27.0	-4.220	2.278	KUR
3873.006	27.0	-4.521	2.278	KUR
3873.010	27.0	-4.056	2.278	KUR
3873.010	27.0	-4.082	2.278	KUR
3873.010	27.0	-4.396	2.278	KUR
3873.017	27.0	-3.799	2.278	KUR
3873.017	27.0	-4.048	2.278	KUR
3873.017	27.0	-4.646	2.278	KUR
3873.026	27.0	-3.583	2.278	KUR

Table A.1 – *Continued*

Wavelength [Å]	Species	log gf	E.P. [eV]	Reference
3873.026	27.0	-4.209	2.278	KUR
3873.026	27.0	-5.074	2.278	KUR
3873.071	27.0	-3.642	0.431	KUR
3873.073	27.0	-3.244	0.431	KUR
3873.075	27.0	-3.040	0.431	KUR
3873.077	27.0	-2.943	0.431	KUR
3873.079	27.0	-2.943	0.431	KUR
3873.082	27.0	-3.098	0.431	KUR
3873.089	27.0	-2.399	0.431	KUR
3873.090	27.0	-2.203	0.431	KUR
3873.092	27.0	-2.098	0.431	KUR
3873.093	27.0	-2.051	0.431	KUR
3873.093	27.0	-2.466	0.431	KUR
3873.095	27.0	-2.057	0.431	KUR
3873.098	27.0	-2.130	0.431	KUR
3873.098	27.0	-2.203	0.431	KUR
3873.100	27.0	-2.341	0.431	KUR
3873.103	27.0	-1.999	0.431	KUR
3873.108	27.0	-1.829	0.431	KUR
3873.114	27.0	-1.683	0.431	KUR
3873.120	27.0	-1.554	0.431	KUR
3873.127	27.0	-1.438	0.431	KUR
3873.133	27.0	-1.333	0.431	KUR
3873.919	27.0	-3.454	0.513	KUR
3873.925	27.0	-3.044	0.513	KUR
3873.930	27.0	-2.822	0.513	KUR
3873.935	27.0	-2.697	0.513	KUR
3873.939	27.0	-2.340	0.513	KUR
3873.940	27.0	-2.646	0.513	KUR
3873.942	27.0	-2.144	0.513	KUR
3873.944	27.0	-2.090	0.513	KUR
3873.944	27.0	-2.676	0.513	KUR
3873.946	27.0	-2.112	0.513	KUR
3873.947	27.0	-2.203	0.513	KUR
3873.947	27.0	-2.391	0.513	KUR
3873.954	27.0	-2.646	0.513	KUR
3873.957	27.0	-2.258	0.513	KUR
3873.959	27.0	-2.003	0.513	KUR
3873.961	27.0	-1.805	0.513	KUR
3873.962	27.0	-1.641	0.513	KUR
3873.963	27.0	-1.500	0.513	KUR
3995.269	27.0	-2.026	0.922	KUR
3995.271	27.0	-1.763	0.922	KUR
3995.271	27.0	-1.959	0.922	KUR
3995.276	27.0	-1.559	0.922	KUR
3995.276	27.0	-1.763	0.922	KUR
3995.276	27.0	-2.658	0.922	KUR
3995.282	27.0	-1.389	0.922	KUR
3995.282	27.0	-1.658	0.922	KUR
3995.282	27.0	-2.503	0.922	KUR
3995.290	27.0	-1.243	0.922	KUR
3995.290	27.0	-1.611	0.922	KUR
3995.290	27.0	-2.503	0.922	KUR
3995.301	27.0	-1.114	0.922	KUR
3995.301	27.0	-1.617	0.922	KUR
3995.301	27.0	-2.600	0.922	KUR
3995.313	27.0	-0.998	0.922	KUR
3995.313	27.0	-1.690	0.922	KUR
3995.313	27.0	-2.804	0.922	KUR
3995.328	27.0	-0.893	0.922	KUR
3995.328	27.0	-1.901	0.922	KUR
3995.328	27.0	-3.202	0.922	KUR
4121.294	27.0	-0.993	0.922	KUR
4121.301	27.0	-1.098	0.922	KUR
4121.308	27.0	-1.214	0.922	KUR
4121.313	27.0	-1.343	0.922	KUR
4121.316	27.0	-2.001	0.922	KUR
4121.318	27.0	-1.489	0.922	KUR

Table A.1 – *Continued*

Wavelength [Å]	Species	log gf	E.P. [eV]	Reference
4121.321	27.0	-1.790	0.922	KUR
4121.322	27.0	-1.659	0.922	KUR
4121.324	27.0	-1.717	0.922	KUR
4121.326	27.0	-1.863	0.922	KUR
4121.327	27.0	-1.711	0.922	KUR
4121.329	27.0	-1.758	0.922	KUR
4121.329	27.0	-2.126	0.922	KUR
4121.331	27.0	-1.863	0.922	KUR
4121.332	27.0	-2.059	0.922	KUR
4121.336	27.0	-2.758	0.922	KUR
4121.336	27.0	-3.302	0.922	KUR
4121.337	27.0	-2.603	0.922	KUR
4121.338	27.0	-2.603	0.922	KUR
4121.338	27.0	-2.700	0.922	KUR
4121.338	27.0	-2.904	0.922	KUR
Ni				
3858.297	28.0	-0.960	0.422	LAW
5139.255	28.0	-1.097	3.655	SNE
5476.904	28.0	-0.780	1.825	LAW
Sr				
4077.709	38.1	0.167	0.000	SNE
4215.519	38.1	-0.145	0.000	SNE
Y				
4374.946	39.1	0.160	0.408	BIE
Ba				
4554.001	56.1	-0.636	0.000	GAL
4554.002	56.1	-1.033	0.000	GAL
4554.002	56.1	-0.636	0.000	GAL
4554.003	56.1	-0.636	0.000	GAL
4554.004	56.1	-1.033	0.000	GAL
4554.004	56.1	-0.636	0.000	GAL
4554.034	56.1	0.170	0.000	GAL
4554.034	56.1	0.170	0.000	GAL
4554.036	56.1	0.170	0.000	GAL
4554.050	56.1	-0.189	0.000	GAL
4554.053	56.1	-0.636	0.000	GAL
4554.053	56.1	-0.189	0.000	GAL
4554.054	56.1	-1.337	0.000	GAL
4554.056	56.1	-0.636	0.000	GAL
4554.057	56.1	-1.337	0.000	GAL
6141.725	56.1	-2.456	0.704	GAL
6141.725	56.1	-2.456	0.704	GAL
6141.727	56.1	-1.311	0.704	GAL
6141.727	56.1	-1.311	0.704	GAL
6141.728	56.1	-2.284	0.704	GAL
6141.728	56.1	-2.284	0.704	GAL
6141.729	56.1	-1.214	0.704	GAL
6141.729	56.1	-0.503	0.704	GAL
6141.729	56.1	-1.214	0.704	GAL
6141.729	56.1	-0.503	0.704	GAL
6141.730	56.1	-0.077	0.704	GAL
6141.730	56.1	-0.077	0.704	GAL
6141.730	56.1	-0.077	0.704	GAL
6141.731	56.1	-1.327	0.704	GAL
6141.731	56.1	-0.709	0.704	GAL
6141.731	56.1	-1.327	0.704	GAL
6141.731	56.1	-0.709	0.704	GAL
6141.732	56.1	-1.281	0.704	GAL
6141.732	56.1	-0.959	0.704	GAL
6141.732	56.1	-0.959	0.704	GAL
6141.733	56.1	-1.281	0.704	GAL
6496.898	56.1	-1.886	0.604	GAL
6496.899	56.1	-1.886	0.604	GAL
6496.901	56.1	-1.186	0.604	GAL
6496.902	56.1	-1.186	0.604	GAL
6496.906	56.1	-0.739	0.604	GAL
6496.906	56.1	-0.739	0.604	GAL
6496.910	56.1	-0.380	0.604	GAL

Table A.1 – *Continued*

Wavelength [Å]	Species	log gf	E.P. [eV]	Reference
6496.910	56.1	-0.380	0.604	GAL
6496.910	56.1	-0.380	0.604	GAL
6496.916	56.1	-1.583	0.604	GAL
6496.916	56.1	-1.583	0.604	GAL
6496.917	56.1	-1.186	0.604	GAL
6496.918	56.1	-1.186	0.604	GAL
6496.920	56.1	-1.186	0.604	GAL
6496.922	56.1	-1.186	0.604	GAL